Mon. Not. R. Astron. Soc. **000**, 000–000 (0000) Printed 26 October 2009 (MN LATEX style file v2.2)

General physical properties of bright Fermi blazars

G. Ghisellini[1⋆], F. Tavecchio[1], L. Foschini[1], G. Ghirlanda[1], L. Maraschi[2], A. Celotti[3]
[1] *INAF – Osservatorio Astronomico di Brera, Via Bianchi 46, I–23807 Merate, Italy*
[2] *INAF – Osservatorio Astronomico di Brera, Via Brera 28, I–20100 Milano, Italy*
[3] *S.I.S.S.A., V. Beirut 2–4, I–34014 Trieste, Italy*

26 October 2009

ABSTRACT
We studied all blazars of known redshift detected by the *Fermi* satellite during its first three–months survey. For the majority of them, pointed *Swift* observations ensures a good multi-wavelength coverage, enabling us to to reliably construct their spectral energy distributions (SED). We model the SEDs using a one–zone leptonic model and study the distributions of the derived interesting physical parameters as a function of the observed γ–ray luminosity. We confirm previous findings concerning the relation of the physical parameters with source luminosity which are at the origin of the blazar sequence. The SEDs allow to estimate the luminosity of the accretion disk for the majority of broad emitting line blazars, while for the line–less BL Lac objects in the sample upper limits can be derived. We find a positive correlation between the jet power and the luminosity of the accretion disk in broad line blazars. In these objects we argue that the jet must be proton–dominated, and that the total jet power is of the same order of (or slightly larger than) the disk luminosity. We discuss two alternative scenarios to explain this result.

Key words: BL Lacertae objects: general — quasars: general — radiation mechanisms: non–thermal — gamma-rays: theory — X-rays: general

1 INTRODUCTION

The Large Area Telescope (LAT) onboard the *Fermi* Satellite, in the first months of operation succeeded to double the number of know γ–ray emitting blazars (Abdo et al. 2009a, hereafter A09). Excluding radio–galaxies, in the list of the LAT 3–months survey we have 104 blazars, divided into 58 Flat Spectrum Radio Quasars (FSRQs, including one Narrow Line Seyfert 1 galaxy), 42 BL Lacs and 4 sources of uncertain classification. Of these, 89 have a known redshift, and a large fraction of sources have been observed with the *Swift* satellite within the 3 months survey, while others have been observed by *Swift* at other epochs.

The combination of *Fermi* and *Swift* data are of crucial importance for the modelling of these blazars, even if the LAT data are an average over the 3 months of the survey, so that, strictly speaking, we cannot have a really simultaneous optical to X–ray SED, even when the *Swift* observations have been performed during the three months of the survey. Despite this, the optical/UV, X–ray and γ–ray coverage can often define or strongly constrain the position and the flux levels of both peaks of the non–thermal emission of blazars. Furthermore, as discussed in Ghisellini, Tavecchio & Ghirlanda (2009, hereafter Paper 1), the data from the UV Optical Telescope (UVOT) of *Swift* are often crucial to disentangle the non–thermal beamed jet emission from thermal radiation produced by the accretion disk. When the accretion disk is visible it is then possible to estimate both the mass of the black hole and the accretion luminosity and to compare it with the power carried by the jet. In Paper I we did this study for the 23 most luminous blazars, exceeding, in the γ–ray range, an observed luminosity of 10^{48} erg s^{-1}. In Tavecchio et al. (2009, hereafter T09) we considered the BL Lac objects detected by *Fermi* with the aim to find, among those, the best candidates to be TeV emitters. Here we extend these previous studies to the entire *Fermi* blazar sample of the 3 months survey. Besides finding the intrinsic physical properties characterising the emitting region of these *Fermi* blazars, like magnetic field, particle density, size, beaming factor and so on, the main goal of our study is to investigate if there is a relation between the jet power and the disk luminosity, as a function of the γ–ray luminosity.

This implies two steps. First we collect the data to construct the SED of all sources, taking advantage of possible *Swift* observations, that we analyse, and of archival data taken from the NASA Extragalactic Database (NED, `http://nedwww.ipac.caltech.edu/`. Secondly, we apply a model to fit these data, that returns the value of the physical parameters of the emitting region, and, if possible, the value of the accretion disk luminosity and of the black hole mass. We do this for all the 85 sources (out of 89) with a minimum coverage of the SED. Among these blazars, there are several BL Lac objects for which there is no sign of thermal emission produced by a disk, nor of emission lines produced by the photo–ionising disk photons. For them we derive an upper limit of the luminosity of a standard, Shakura–Sunyaev (1973) disk. We also derive the distri-

⋆ Email: gabriele.ghisellini@brera.inaf.it

butions of the needed physical parameters, and their dependence on the γ–ray luminosity and on the presence/absence of a prominent accretion disk. As expected, the jets of line–less BL Lacs have less power than broad line FSRQs, have bluer spectra, and their emitting electrons suffer less radiative cooling. This confirms earlier results (Ghisellini et al. 1998) explaining the so called blazar sequence (Fossati et al. 1998).

The main result of our analysis concerns the relation between the jet power and the accretion disk luminosity. We find that they correlate in FSRQs, for which we can estimate both the black hole mass and the accretion luminosity. We discuss two alternative scenarios to explain this behaviour. For BL Lacs (with only an upper limit on the accretion luminosity), we suggest that the absence of any sign of thermal emission, coupled to the presence of a relatively important jet, strongly suggests a radiatively inefficient accretion regime.

In this paper we use a cosmology with $h = \Omega_\Lambda = 0.7$ and $\Omega_{\rm M} = 0.3$, and use the notation $Q = Q_X 10^X$ in cgs units (except for the black hole masses, measured in solar mass units).

2 THE SAMPLE

Tab. 1 lists the 89 blazars with redshift of the A09 catalogue of *Fermi* detected blazars. Besides their name, we report the redshift, the K–corrected γ–ray luminosity in the *Fermi*/LAT band, (see e.g. Ghisellini, Maraschi & Tavecchio 2009), if there are observations by the *Swift* satellite, if the source was detected by EGRET and the classification. For the latter item we have maintained the same classification as in A09, but we have indicated those sources classified as BL Lac objects but that do have broad emission lines.

The distinction between BL Lacs and FSRQs is traditionally based on the line equivalent width (EW) being smaller or larger than 5Å. With this definition, we classify as BL Lacs those sources having genuinely very weak or absent lines and also objects with strong lines but whose non–thermal continuum is so enhanced to reduce the line EW. This second category of "BL Lacs" should physically be associated to FSRQs. We have tentatively made this distinction on Tab. 1, based on some information from the literature about the presence, in these objects, of strong broad lines. In the rest of the paper we will consider them as FSRQs.

The source PMN 0948–0022 belongs to still another class, being a Narrow Line Seyfert 1 (NLSy1; FWHM$\sim$1500 km s^{-1}). This source has been discussed in detail in Abdo et al. (2009b) and Foschini et al. (2009): its SED and general properties are indistinguishable from FSRQs and we then assign this source to this group.

We then have 57 FSRQs, 1 NLSy1 and 31 BL Lac objects. Of the latter, 6 have strong broad lines or have been also classified as FSRQs (by Jauncey et al. 1989). Four of the FSRQs (indicated with the superscript n in Table 1) do not have a sufficient data coverage to allow a meaningful interpretation, and we will not discuss them. The 23 blazars (21 FSRQs and 2 BL Lacs, but with broad emission lines) with an average γ–ray luminosity exceeding 10^{48} erg s^{-1} written in italics have been discussed in Paper 1. The 25 underlined BL Lacs are discussed in T09. One of these, (0814+425=OJ 425) is shown also here, since it can be fitted both with a pure synchrotron self–Compton (SSC) and an "External Compton" (EC) model (see next section).

In summary, in this paper we present the SED and the corresponding models for 37 blazars: 32 FSRQs and 5 BL Lacs that are suspected to be FSRQs with broad lines hidden by the beamed continuum. However, when discussing the general properties of the *Fermi* blazars, we will consider the entire blazar sample of Tab. 1, with the only exception of the 4 FSRQs with a very poor data coverage. These are 85 sources. To this aim we will use the results of Paper 1, concerning the most γ–ray luminous blazars, and we will apply our model also to the BL Lacs shown in T09. For the ease of the reader, we report in Table 4 and Table 5 the physical parameters of all the 85 blazars.

Name	Alias	z	log L_γ	*S?*	E?	Type
0017–0512^n	CGRaBS	0.227	45.96	Y	Y	Q
00311–1938	KUV	0.610	46.40	Y		B
0048–071	*PKS*	1.975	48.2			Q
0116–219	PKS	1.165	47.68			Q
0118–272	PKS	0.559	46.48		UL	B
0133+47	DA 55	0.859	47.41	Y	UL	Q
0142–278	PKS	1.148	47.63			Q
0202–17	*PKS*	1.74	48.2		UL	Q
0208–512	PKS	1.003	47.92	Y	Y	Q
0215+015	*PKS*	1.715	48.16	Y	UL	Q
0218+35	B2	0.944	47.47	Y	UL	Q
0219+428	3C66A	0.444	47.16	Y	Y	B
0227–369	*PKS*	2.115	48.6	Y		Q
0235+164	*AO*	0.94	48.4	Y	Y	B*
0301–243	PKS	0.260	45.77	Y	UL	B
0332–403	PKS	1.445^b	47.68	Y	UL	B**
0347–211	*PKS*	2.944	49.1	Y		Q
0426–380	*PKS*	1.112	48.06	Y	UL	B*
0447–439	PKS	0.107	46.03	Y		B
0454–234	*PKS*	1.003	48.16	Y	Y	Q
0502+675	1ES	0.314	46.06	Y		B
0528+134	*PKS*	2.04	48.8	Y	Y	Q
0537–441	PKS	0.892	47.99	Y	Y	B*
0650+453	B3	0.933	47.82	Y		Q
0713+1935^n	CLASS	0.534	46.84			Q
0716+332	TXS	0.779	47.12	Y		Q
0716+714	TXS	0.26	46.55	Y	Y	B
0735+178	PKS	0.424	46.31	Y	Y	B
0814+425	OJ 425	0.53	46.87	Y	UL	B
0820+560	*S4*	1.417	48.01	Y		Q
0851+202	OJ 287	0.306	46.18	Y	UL	B
0917+449	*TXS*	2.1899	48.4	Y	Y	Q
0948+0022	PMN	0.585	46.95	Y		NL^a
0954+556	4C 55.17	0.8955	47.41	Y	Y	Q
1011+496	1ES	0.212	45.83	Y		B
1012+2439^n	CRATES	1.805	47.99			Q
1013+054	*TXS*	1.713	48.2			Q
1030+61	S4	1.401	47.87	Y		Q
1050.7+4946	MS	0.140	44.65	Y		B
1055+018	PKS	0.89	47.11	Y	UL	Q
1057–79	PKS	0.569	47.06	Y	UL	B**
10586+5628	RX	0.143	45.14			B
1101+384	Mkn 421	0.031	44.52	Y	Y	B

Table 1. The 89 *Fermi* blazars in the A09 catalogue with redshift, including two blazars that have no z in the A09 lists (0332–403 and 1553+11). In the last 4 columns we indicate the logarithm of the average γ–ray luminosity as observed by *Fermi* during the first 3 months of survey (cgs units); if there are *Swift* observations; if the source was detected by EGRET (UL stands for an upper limit given by Fichtel et al. 1994); the classification of the source (B=BL Lac; Q=FSRQs; NL=Narrow line Seyfert galaxy; U=uncertain classification). a: Narrow Line Seyfert 1, analysed in Abdo et al. (2009b) and Foschini et al. (2009). b: redshift uncertain. n: not studied in this paper due to lack of multiwavelength data; $*$: defined as BL Lacs for the EW of the lines, but broad emission lines are present. $**$: classified as FSRQ in Jauncey et al. (1989).

Name	Alias	z	$\log L_\gamma$	*S?*	E?	Type
1127–145	PKS	1.184	47.70	Y	Y	Q
1144–379	PKS	1.049	47.35	Y	UL	Q
1156+295	4C 29.45	0.729	47.15	Y	Y	Q
1215+303	B2	0.13	45.57		UL	B
1219+285	ON 231	0.102	45.25	Y	Y	B
1226+023	3C 273	0.158	46.33	Y	Y	Q
1244–255	PKS	0.635	46.86	Y	UL	Q
1253–055	3C 279	0.536	47.31	Y	Y	Q
1308+32	B2	0.996	47.72	Y	UL	Q
1329–049	*PKS*	2.15	48.5			Q
1333+5057^n	CLASS	1.362	47.73			Q
1352–104	PKS	0.332	46.17		UL	Q
1454–354	*PKS*	1.424	48.5	Y	Y	Q
1502+106	*PKS*	1.839	49.1	Y	UL	Q
1508–055	PKS	1.185	47.65	Y	UL	Q
1510–089	PKS	0.360	47.10	Y	Y	Q
1514–241	Ap Lib	0.048	44.25	Y	Y	B
1520+319	*B2*	1.487	48.4	Y		Q
1551+130	*PKS*	1.308	48.04			Q
1553+11	PG	0.36^b	46.57	Y		B
1622–253	PKS	0.786	47.44		Y	Q
1633+382	*4C+38.41*	1.814	48.6	Y	Y	Q
1652+398	Mkn 501	0.0336	43.95	Y	Y	B
1717+177	PKS	0.137	45.50	Y	UL	B
1749+096	OT 081	0.322	46.56	Y	UL	B
1803+784	S5	0.680	46.88	Y	UL	B*
1846+322	TXS	0.798	47.42	Y		Q
1849+67	S4	0.657	47.29	Y		Q
1908–201	PKS	1.119	47.99	Y	Y	Q
1920–211	TXS	0.874	47.49	Y	Y	Q
1959+650	1ES	0.047	44.30	Y		B
2005–489	PKS	0.071	44.51	Y	Y	B
2023–077	*PKS*	1.388	48.6	Y	Y	Q
2052-47	*PKS*	1.4910	48.03		Y	Q
2141+175	OX 169	0.213	45.93	Y	UL	Q
2144+092	PKS	1.113	47.85	Y	UL	Q
2155–304	PKS	0.116	45.76	Y	Y	B
2155+31	B2	1.486	47.84	Y		Q
2200+420	BL Lac	0.069	44.74	Y	Y	B
2201+171	PKS	1.076	47.45	Y	UL	Q
2204–54	PKS	1.215	47.80	Y	UL	Q
2227–088	*PHL 5225*	1.5595	48.2	Y	UL	Q
2230+114	CTA102	1.037	47.69	Y	Y	Q
2251+158	*3C 454.3*	0.859	48.7	Y	Y	Q
2325+093	*PKS*	1.843	48.5	Y		Q
2345–1555	PMN	0.621	46.99	Y		Q

Table 1. – continue –

3 SWIFT OBSERVATIONS AND ANALYSIS

For 33 of the 37 blazars studied in this paper there are *Swift* observations, with several of them being observed during the 3 months of the *Fermi* survey. The data were analysed with the most recent software `SWIFT_REL3.2` released as part of the `Heasoft v. 6.6.2`. The calibration database is that updated to April 10, 2009. The XRT data were processed with the standard procedures (`XRTPIPELINE v.0.12.2`). We considered photon counting (PC) mode data with the standard 0–12 grade selection. Source events were extracted in a circular region of aperture $\sim 47''$, and background was estimated in a same sized circular region far from the source. Ancillary response files were created through the `xrtmkarf` task. The channels with energies below 0.2 keV and above 10 keV were excluded from the fit and the spectra were rebinned in energy so to have at least 30 counts per bin. Each spectrum was analysed through XSPEC with an absorbed power–law with a fixed Galactic column density from Kalberla et al. (2005). The computed errors represent the 90% confidence interval on the spectral parameters. Tab. 2 reports the log of the observations and the results of the fitting the X–ray data with a simple power law model.

UVOT (Roming et al. 2005) source counts were extracted from a circular region $5''-$sized centred on the source position, while the background was extracted from a larger circular nearby source–free region. Data were integrated with the `uvotimsum` task and then analysed by using the `uvotsource` task. The observed magnitudes have been dereddened according to the formulae by Cardelli et al. (1989) and converted into fluxes by using standard formulae and zero points from Poole et al. (2008). Tab. 3 list the observed magnitudes in the 6 filters of UVOT.

4 THE MODEL

We use the model described in detail in Ghisellini & Tavecchio (2009, hereafter GT09). It is a relatively simple, one zone, homogeneous synchrotron and Inverse Compton model, aiming at accounting the several contributions to the radiation energy density produced externally to the jet, and their dependence upon the distance of the emitting blob to the black hole. Besides the synchrotron radiation produced internally to the jet, we in fact consider radiation coming directly from the disk (i.e. Dermer & Schlickeiser 1993), the broad line region (BLR; e.g. Sikora, Begelman & Rees 1994), a dusty torus (see Błazejowski et al. 2000; Sikora et al. 2002), the host galaxy light and the cosmic background radiation.

The emitting region is assumed spherical, of size $r_{\rm diss}$, moving with a bulk Lorentz factor Γ and is located at a distance $R_{\rm diss}$ from the black hole of mass M. The bolometric luminosity of the accretion disk is $L_{\rm d}$. The jet accelerates in its inner parts with $\Gamma \propto R^{1/2}$ (R is the distance from the black hole), up to a value $\Gamma_{\rm max}$. In the acceleration region the jet is parabolic (following, e.g. Vlahakis & Königl 2004) and beyond this point the jet becomes conical with a semi–aperture angle ψ (assumed to be 0.1 for all sources).

The energy particle distribution $N(\gamma)$ [cm^{-3}] is calculated solving the continuity equation where particle injection, radiative cooling and pair production (via the γ–$\gamma \to e^{\pm}$ process) are taken into account. The injection function $Q(\gamma)$ [cm^{-3} s^{-1}] is assumed to be a smoothly joining broken power–law, with a slope $Q(\gamma) \propto \gamma^{-s_1}$ and γ^{-s_2} below and above a break energy $\gamma_{\rm b}$:

$$Q(\gamma) \, = \, Q_0 \, \frac{(\gamma/\gamma_{\rm b})^{-s_1}}{1+(\gamma/\gamma_{\rm b})^{-s_1+s_2}} \qquad (1)$$

The total power injected into the source in the form of relativistic electrons is $P'_{\rm i} \, = \, m_{\rm e}c^2 V \int Q(\gamma)\gamma d\gamma$, where $V \, = \, (4\pi/3) r^3_{\rm diss}$ is the volume of the emitting region.

The injection process lasts for a light crossing time $r_{\rm diss}/c$, and we calculate $N(\gamma)$ at this time. This assumption comes from the fact that even if injection lasted longer, adiabatic losses caused by the expansion of the source (which is travelling while emitting) and the corresponding decrease of the magnetic field would make the observed flux to decrease. Therefore our calculated spectra correspond to the maximum of a flaring episode.

The BLR is assumed for simplicity to be a thin spherical shell located at a distance $R_{\rm BLR} \, = \, 10^{17} L^{1/2}_{\rm d,45}$ cm. A fraction

source	Obs. date dd/mm/yyyy	$N_{\rm H}^{\rm Gal}$ 10^{20} cm^{-2}	Γ	$\chi 2/{\rm dof}$	$F_{0.2-10,{\rm unabs}}$ 10^{-12} cgs	$F_{2-10,{\rm unabs}}$ 10^{-12} cgs
0133+47*	18/11/2008	11.4	1.4±0.2	19/13	3.72±0.43	2.57±0.33
0208–512*	29/12/2008	3.19	1.9±0.2	6/11	2.6±0.3	1.26±0.2
0218+35*	12/12/2008	5.86	$2.7^{+1.1}_{-1.0}$	0.2/3	2.0±0.4	0.29±0.05
0332–403(^{a})	25/02/2009	1.38	1.4±0.2	2/6	3.5±0.4	2.4±0.2
0537–441	08/10/2008	3.94	1.7±0.1	23/20	8.24±0.9	4.63±0.47
0650+453*	14/02/2009	8.64	2.1±0.6	5/5	0.76±0.11	0.28±0.04
0716+332	27/01/2008	5.93	1.8±0.3	3/3	0.9±0.2	0.4±0.2
0948+0022**	05/12/2008	5.22	1.8±0.2	5/8	4.4±0.2	2.2±0.1
0954+556	05/03/2009	0.853	$0.9^{+1.1}_{-1.8}$	0.1/2	2.2±0.5	1.9±0.5
1030+61*	03/07/2009	0.63	1.9±0.7	0.3/4	0.62±0.10	0.27±0.04
1055+018*	19/07/2008	4.02	1.8±0.5	1/3	3.5	1.8
1057–79	20/01/2008	8.76	1.9±0.15	6/10	2.8±0.4	1.3±0.3
1127–145	24/03/2007	4.04	1.31±0.05	116/94	9.8±0.5	7.2±0.4
1144–379*	21/11/2008	7.5	1.96±0.32	1/5	1.0±0.3	0.46±1.2
1156+295	21/11/2008	1.68	1.52±0.14	11/7	2.7±0.4	1.7±0.2
1226+023	10/05/2008	1.79	1.56±0.05	88/68	833±19	521±26
1244–255	17/01/2007	6.85	1.8±0.5	3/4	2.1±0.5	1.0±0.4
1253–055(^{b})	08/08/2008	2.12	1.76±0.04	88/94	10.5±0.2	5.5±0.1
1308+32	20/08/2008	1.27	1.6±0.2	5/10	3.0±0.2	1.8±0.1
1508–055(^{c})	20/02/2007	6.09	1.8±0.2	8/6	0.95±0.08	0.50±0.04
1510–089	10/01/2009	7.8	1.4±0.11	194/316	6.4±1.3	4.4±0.4
1803+784	17/02/2007	4.12	1.5±0.1	14/14	2.8±0.4	1.8±0.2
1846+322(^{d})	28/12/2008	9.93	1.7±0.2	10/7	0.78±0.05	0.45±0.03
1849+67(^{e})	16/11/2006	4.66	1.5±0.1	22/14	2.6±0.1	1.59±0.07
1908–201(^{f})	08/03/2007	9.24	1.4±0.1	5/10	2.7±0.1	1.83±0.05
1920–211	07/08/2007	5.69	1.6±0.3	1/3	1.4±0.1	0.87±0.09
2141+175(^{g})	19/04/2007	7.35	1.71±0.06	94/67	2.23±0.04	1.47±0.03
2144+092(^{h})	28/04/2009	4.56	1.6±0.2	13/9	1.6±0.1	1.01±0.07
2155+31(^{i})	01/04/2009	7.42	1.0±0.6	0.6/1	1.0±0.1	0.8±0.1
2201+171(^{l})	08/12/2009	4.56	$1.80^{+0.08}_{-0.15}$	13/17	1.22±0.05	0.62±0.03
2204–54	21/12/2008	1.72	1.6±0.1	9/17	2.2±0.1	1.37±0.07
2230+114(^{m})	19/05/2005	4.76	1.50±0.05	74/66	6.5±0.1	4.2±0.1
2345–155(^{n})	23/12/2008	1.64	1.6±0.4	0.3/1	0.39±0.05	0.23±0.03

Table 2. Results of the X–ray analysis. *: poorly determined spectrum, the C–Statistic was used to fit the spectrum. Therefore, the $\chi 2/{\rm dof}$ indicates instead the C-stat value and the PHA bins. ** Abdo et al. (2009b). *a:* Average of 2 observations the same day. *b:* Average of 8 observations between 8 and 20 August 2008. *c:* Average of 4 observations between 26/02/2007 and 13/09/2008. *d:* Average of 2 observations on 28/12/2008 and 20/02/2009. *e:* Average of 3 observations between 16/11/2006 and 04/08/2008. *f:* Average of 4 observations between 8 and 17 March 2007. *g:* Average of 9 observations between 19/04/2007 and 15/01/2009. *h:* Average of 2 observations the same day. *i:* Average of 3 observations between 1 and 17 April 2009. *l:* Average of 7 observations between 08/12/2006 and 18/04/2009. *m:* Average of 5 observations between 19/05/2005 and 01/05/2007. *n:* Average of 2 observations on 23/12/2008 and 10/01/2009.

$f_{\rm BLR}=0.1$ of the disk luminosity is re–emitted by broad lines. Since $R_{\rm BLR}\propto L_{\rm d}^{1/2}$, the radiation energy density of the broad line emission within the BLR is constant, but is seen amplified by a factor $\sim\Gamma^2$ by the moving blob, as long as $R_{\rm diss}<R_{\rm BLR}$. A dusty torus, located at a distance $R_{\rm IR}=2.5\times 10^{18}L_{\rm d}^{1/2}$ cm, reprocesses a fraction $f_{\rm IR}$ (of the order of 0.1–0.3) of $L_{\rm d}$ through dust emission in the far IR. Above and below the accretion disk, in its inner parts, there is an X–ray emitting corona of luminosity $L_{\rm X}$ (we almost always fixes it at a level of 30% of $L_{\rm d}$). Its spectrum is a power law of energy index $\alpha_X=1$ ending with a exponential cut at $E_{\rm c}$ =150 keV. The specific energy density (i.e. as a function of frequency) of all these external components are calculated in the comoving frame, and used to properly calculate the resulting External inverse Compton (EC) spectrum. The internally produced synchrotron emission is used to calculate the synchrotron self Compton (SSC) flux.

5 SOME GUIDELINES FOR THE MODELLING

In this section we follow (and somewhat repeat) the arguments presented in Paper 1, adding some considerations for line–less BL Lac objects.

A general comment concerns the flux at low (sub–mm to radio) frequencies. The one–zone homogeneous model here adopted is aimed to explain the bulk of the emission, and necessarily requires a compact source, self–absorbed (for synchrotron) at $\sim 10^{12}$ Hz. The flux at radio frequencies must be produced further out in the jet. Radio data, therefore, are not directly constraining the model. Indirectly though, they can suggest a sort of continuity between the level of the radio emission and what the model predicts at higher frequencies.

5.1 Strong line objects

Consider first sources whose inverse Compton flux is dominated by the EC process with photons of the broad line region.

source	OBS date	V	B	U	$W1$	$M2$	$W2$
0133+47	18/11/2008	15.89±0.02	16.46±0.01	15.89±0.01	16.30±0.02	16.56±0.03	16.74±0.02
0208–512	29/12/2008	17.69±0.07	18.06±0.05	17.01±0.04	16.79±0.03	16.69±0.03	17.03±0.03
0218+35	12/12/2008	>19.4	>20.3	>19.9	>20.3	>20.1	>21.0
0332–403	25/02/2009	17.00±0.07	17.59±0.05	16.85±0.05	17.23±0.06	17.29±0.07	18.20±0.07
0537–441	08/10/2008	16.04±0.02	16.48±0.02	15.78±0.02	16.01±0.02	16.02±0.02	16.26±0.02
0650+453	14/02/2009	>19.8	20.1±0.2	19.3±0.2	19.3±0.1	19.4±0.1	19.8±0.1
0716+332	27/01/2008	–	–	–	–	–	17.71±0.03
0948+0022*	05/12/2008	18.2±0.2	18.56±0.07	17.79±0.06	17.48±0.06	17.50±0.06	17.55±0.05
0954+556	05/03/2009	17.6±0.2	17.97±0.06	16.91±0.04	16.80±0.04	16.8±0.2	16.94±0.08
1030+61	03/07/2009	18.4±0.1	19.14±0.08	18.36±0.07	18.56±0.07	18.5±0.1	19.08±0.08
1055+018	19/07/2008	–	–	–	–	16.97±0.04	–
1057–79	20/01/2008	–	–	–	–	17.31±0.03	17.36±0.01
1127–145	24/03/2007	16.46±0.02	16.70±0.01	15.64±0.01	15.51±0.01	15.55±0.01	15.79±0.01
1144–379	21/11/2008	–	–	–	–	–	20.0±0.1
1156+295	21/11/2008	–	–	–	16.85±0.01	–	–
1226+023	10/05/2008	12.72±0.01	12.92±0.01	11.92±0.01	11.48±0.01	11.33±0.01	11.34±0.01
1244–255	17/01/2007	–	–	–	–	17.44±0.03	–
1253–055	08/08/2008	16.80±0.09	16.25±0.06	16.41±0.05	16.44±0.05	16.35±0.06	16.50±0.04
1308+32	20/08/2008	–	–	–	–	16.71±0.03	–
1508–055	20/02/2007	17.4±0.2	17.5±0.1	16.56±0.06	16.38±0.09	16.8±0.2	16.97±0.09
1510–089	10/01/2009	16.76±0.08	17.04±0.04	16.18±0.02	16.51±0.02	16.42±0.04	16.52±0.03
1803+784	17/02/2007	16.51±0.03	16.99±0.02	16.32±0.02	16.50±0.02	16.55±0.02	16.65±0.01
1846+322	28/12/2008	18.9±0.1	19.27±0.09	18.50±0.07	18.41±0.06	18.45±0.06	18.62±0.05
1849+67	16/11/2006	17.6±0.1	17.93±0.06	17.28±0.06	17.36±0.06	16.13±0.03	–
1908–201	08/03/2007	16.8±0.1	17.40±0.09	16.80±0.08	17.09±0.09	17.34±0.08	17.66±0.09
1920–211	07/08/2007	–	–	–	16.73±0.03	–	–
2141+175	19/04/2007	16.16±0.02	16.39±0.02	15.21±0.02	–	15.09±0.03	15.12±0.03
2144+092	28/04/2009	18.2±0.2	18.48±0.09	17.67±0.07	17.50±0.06	17.68±0.07	18.00±0.05
2155+31	01/04/2009	–	–	–	21.4±0.4	–	> 20.9
2201+171	08/12/2009	16.93±0.06	17.71±0.05	17.23±0.04	17.62±0.05	17.7±0.1	17.86±0.05
2204–54	21/12/2008	17.89±0.08	18.18±0.04	16.98±0.03	16.83±0.03	16.99±0.04	17.40±0.04
2230+114	19/05/2005	–	–	16.52±0.02	–	16.38±0.04	16.70±0.03
2345–155	23/12/2008	18.5±0.1	18.61±0.06	17.91±0.05	17.57±0.07	17.66±0.05	17.78±0.04

Table 3. UVOT Observed magnitudes. * see also Abdo et al. (2009b) and Foschini et al. (2009).

• When the UVOT data define an optical–UV bump, we interpret it as the direct emission from the accretion disc. This assumption allows us to determine both the black hole mass and the accretion rate. The maximum temperature (and hence the νF_ν peak of the disk luminosity) occurs at ∼5 Schwarzschild radii and scales as $T_{\rm max} \propto (L_{\rm d}/L_{\rm Edd})^{1/4} M^{-1/4}$. The total optical–UV flux gives $L_{\rm d}$ [that of course scales as $(L_{\rm d}/L_{\rm Edd})\, M$]. Therefore we can derive both the black hole mass and the accretion rate. For good UVOT data, the method is sensitive to variations of less than a factor 2 in both the black hole mass and the accretion rate (see the discussion and Fig. 2 in Ghisellini et al. 2009a).

• The ratio between the high to low energy emission humps ($L_{\rm C}/L_{\rm S}$) is directly related to the ratio between the radiation to magnetic energy density $U'_{\rm r}/U'_{\rm B}$. In this case the assumption $R_{\rm BLR} = 10^{17} L_{\rm d,45}^{1/2}$ cm gives

$$\frac{U'_{\rm r}}{U'_{\rm B}} = \frac{L_{\rm C}}{L_{\rm S}} \rightarrow U'_{\rm B} = \frac{L_{\rm S}}{L_{\rm C}} \frac{\Gamma^2}{12\pi} \rightarrow B = \Gamma \left(\frac{2L_{\rm s}}{3L_{\rm C}}\right)^{1/2} \quad (2)$$

where we have assumed that $U'_{\rm r} \approx U'_{\rm BLR}$.

• The peak of the high energy emission ($\nu_{\rm C}$) is produced by the scattering of the line photons (mainly hydrogen Lyman–α) with electrons at the break of the particle distribution ($\gamma_{\rm peak}$). Its observed frequency is $\nu_{\rm C} \sim 2\nu_{Ly\alpha} \Gamma \delta \gamma^2_{\rm peak}/(1+z)$. A steep (energy spectral index $\alpha > 1$) spectrum indicates a peak at energies below 100 MeV, and this constrains $\Gamma\delta\gamma^2_{\rm peak}$.

• Several sources whose Compton flux is dominated by the EC component may have rather small values of $\gamma_{\rm peak}$. Electrons with these energies may emit, by synchrotron, in the self–absorbed regime. In these cases the peak of the synchrotron component is the self–absorption frequency.

• In powerful blazars the radiative cooling rate is almost complete, namely even low energy electrons cool in a dynamical timescale $r_{\rm diss}/c$. We call $\gamma_{\rm cool}$ the random Lorentz factor of those electrons halving their energies in a timescale $r_{\rm diss}/c$. When the EC process dominates, $\gamma_{\rm cool}$ is small (a few). Therefore the corresponding emitting particle distribution is weakly dependent of the low energy spectral slope, s_1, of the injected electron distribution.

• The strength of the SSC relative to the EC emission depends on the ratio between the synchrotron over the external radiation energy densities, as measured in the comoving frame, $U'_{\rm s}/U'_{\rm ext}$. Within the BLR, $U'_{\rm ext}$ depends only on Γ^2, while $U'_{\rm s}$ depends on the injected power, the size of the emission, and the magnetic field. The larger the magnetic field, the larger the SSC component. The shape of the EC and SSC emission is different: besides the fact that the seed photon distributions are different, we have that the flux at a given X–ray frequency is made by electron of very different energies, thus belonging to a different part of the electron distribution.

In this respect, the low frequency X–ray data of very hard X–ray spectra are the most constraining, since in these cases the (softer) SSC component must not exceed what observed. This limits the magnetic field, the injected power (as measured in the comoving frame) and the size. Conversely, a relatively soft spectrum (but still rising, in νF_ν) indicates a SSC origin, and this constrains the combination of B, $r_{\rm diss}$ and $P'_{\rm i}$ even more.

5.2 Line–less BL Lacs

When the SED is dominated by the SSC process, as discussed by Tavecchio et al. (1998), the number of observables (peak fluxes and frequencies of both the synchrotron and SSC components, spectral slopes before and after the peaks, variability timescale) is sufficient to fix all the model parameters. The sources whose high energy emission is completely dominated by the SSC process are line–less BL Lac objects, with less powerful and less luminous jets. The lack of external photons and the weaker radiation losses make $\gamma_{\rm cool}$ much larger in these sources than in FSRQs. The low energy slope of the injected electrons, s_1, in these cases coincides with the low energy slope of the emitting distribution of electrons.

5.3 Upper limits to the accretion luminosity and mass estimate

For line–less BL Lac objects we find an upper limit to the accretion disk luminosity by requiring that the emission directly produced by the disk and by the associated emission lines are completely hidden by the non–thermal continuum. By assuming a typical equivalent width of the emission lines observed in FSRQs (~ 100 Å), and the one defining BL Lacs (EW<5Å), we require that the disk luminosity is a factor at least ~ 20 below the observed non–thermal luminosity. Note that we *assume* that the disk is a standard Shakura & Sunyaev (1973) geometrically thin optically thick disk. That this is probably *not* the case will be discussed later.

A crude estimate of the black hole mass is obtained in the following way. Assume that the dissipation region, in units of Schwarzschild radii, is the same in BL Lacs and FSRQs. Then an *upper limit* to the mass is derived assuming that light crossing times do not exceed the typical variability timescales observed. A *lower limit* can be derived by considering the value of the magnetic field in the emitting region. Small black hole masses imply smaller dimensions, thus smaller Poynting flux (for a given B–field). To avoid implausibly small values of it, we then derive a lower limit to the black hole mass. Together, this two conditions give masses in the range $10^8 - 10^9\ M_\odot$. As we discuss later (§6.1 and Tab. 6), for BL Lacs in which independent mass estimates are available in literature, the masses derived in this way agree quite well.

6 RESULTS

In Fig. 1 and Fig. 2 we show the distributions of the parameters derived from model fitting the SED of the entire sample of *Fermi* blazars (85 sources). Shaded areas in these histograms correspond to the 25 BL Lacs for which only an upper limit to the accretion luminosity could be derived (the plotted areas correspond to 26 objects because they include two states of PKS 2155–304). They can be considered as "genuine" BL Lacs, namely blazars whose emission lines are intrinsically weak or absent, and not hidden by the beamed continuum.

The SED of the 37 blazar studied in this paper, together with the best fitting model, are shown in Figs. 11–20 of the Appendix. In Tab. 2 and Tab. 3 we list the result of our XRT and UVOT analysis for the 33 blazars (out of the 37 blazars studied in this paper) with *Swift* data. All optical–UV fluxes shown in Fig. 11 – 20 have been de–reddened according to the Galactic $A_{\rm V}$ given in the NED database.

Tab. 4 reports the parameters used to compute the theoretical SEDs and Tab. 5 lists the power carried by the jet in the form of radiation, electrons, magnetic field and protons (assuming one pro-

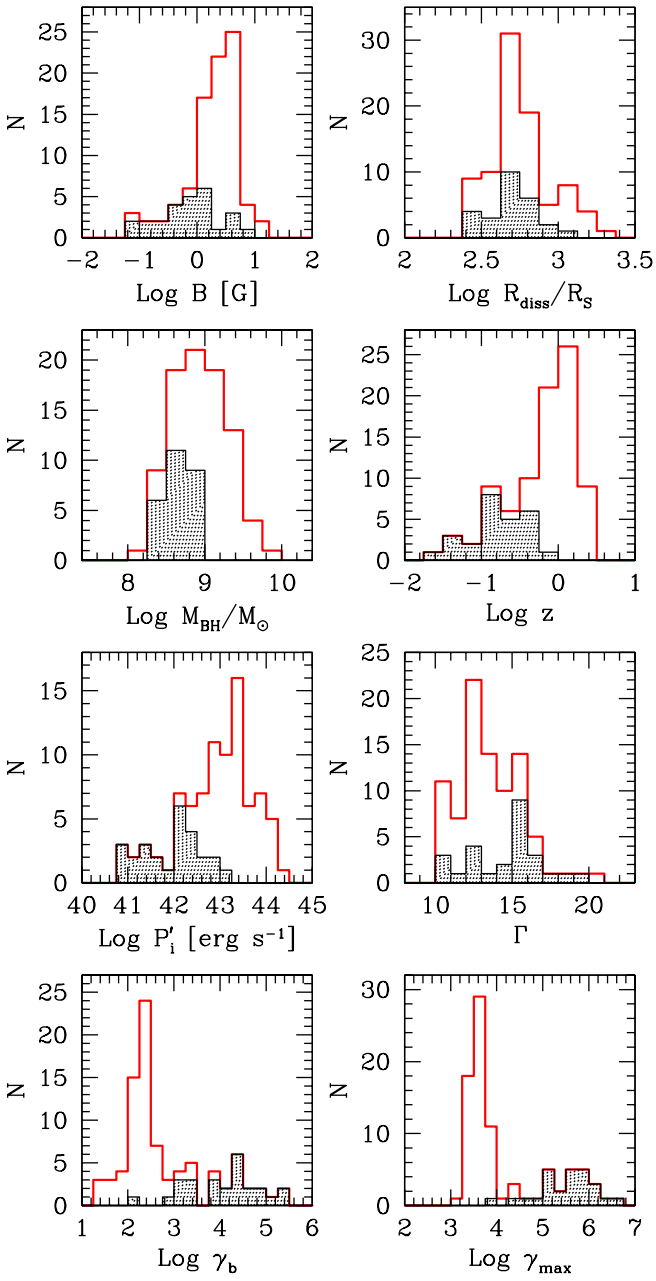

Figure 1. Distribution of the magnetic field, location of the dissipation region in units of the Schwarzschild radius, black hole mass, redshift, power $P'_{\rm i}$ injected in relativistic electrons (as measured in the comoving frame), bulk Lorentz factor, break energy ($\gamma_{\rm b}$) and maximum energy ($\gamma_{\rm max}$) of the injected distribution of electrons for all the 85 blazars. Shaded areas correspond to BL Lacs with only an upper limit on their disk accretion luminosity.

Name [1]	z [2]	$R_{\rm diss}$ [3]	M [4]	$R_{\rm BLR}$ [5]	$P'_{\rm i}$ [6]	$L_{\rm d}$ [7]	B [8]	Γ [9]	$\theta_{\rm v}$ [10]	γ_0 [11]	$\gamma_{\rm b}$ [12]	$\gamma_{\rm max}$ [13]	s_1 [14]	s_2 [15]
00311–1938	0.610	72 (300)	8e8	<33	1.1e–3	<0.11 (<9e–4)	1.7	15	3	1	1.6e4	1e6	0.5	3
0048–071	1.975	210 (700)	1e9	474	0.025	22.5 (0.15)	2.4	15.3	3	1	400	7e3	1	2.7
0116–219	1.165	156 (650)	8e8	310	7e-3	9.6 (0.08)	2.4	14.7	3	1	300	3.5e3	0.5	2.5
0118–272	0.559	75 (500)	5e8	<12	1.2e–3	<0.015 (<2.e–4)	0.75	12.9	3	200	1.5e4	5e5	1	3.2
0133+47	0.859	180 (600)	1e9	387	0.013	15 (0.1)	11.1	13	3	1	20	2.5e3	1	1.9
0142–278	1.148	90 (500)	6e8	268	0.02	7.2 (0.08)	3.91	12.9	3	1	100	3.5e3	1	2.8
0202–17	1.74	300 (1000)	1e9	671	0.03	45 (0.3)	2.4	15	3	1	300	5e3	1	3.1
0208–512	1.003	126 (600)	7e8	383	0.03	14.7 (0.14)	2.05	10	3	1	200	8e3	0	2.5
0215+015	1.715	900 (1500)	2e9	548	0.04	30 (0.1)	1.1	13	3	1	2.5e3	6e3	–1	3.5
0218+35	0.944	54 (450)	4e8	77	0.014	0.6 (0.01)	2.24	12.2	3	1	150	3e3	0	3.2
0219+428	0.444	60 (500)	4.e8	<35	9e–3	<0.12 (<2e–3)	2.3	12.9	3	1	3.1e4	1.5e5	1.1	4.3
0227–369	2.115	420 (700)	2e9	547	0.08	30 (0.1)	1.5	14	3	1	200	5e3	0	3.1
0235+164	0.94	132 (440)	1e9	212	0.042	4.5 (0.03)	2.9	12.1	3	1	400	2.7e3	–1	2.1
0301–243	0.260	144 (600)	8e8	<11	4.8e–4	<0.012 (<1e–4)	0.42	14	3	1	9e3	6e5	1	3.2
0332–403	1.445	450 (300)	5e9	775	0.03	60 (0.08)	4.25	10	3	1	90	3e3	1	2.2
0347–211	2.944	750 (500)	5e9	866	0.12	75 (0.1)	1.5	12.9	3	1	500	3e3	–1	3.0
0426–380	1.112	156 (1300)	4e8	600	0.018	36 (0.6)	1.7	13	3	1	300	6e3	–1	2.4
0447–439	0.107	72 (400)	6e8	<25	1.4e–4	<0.063 (<7e–4)	0.9	15	3	1	2e4	4e5	1	3.5
0454–234	1.003	338 (450)	2.5e9	433	0.027	18.8 (0.05)	3	12.2	3	1	330	4e3	–1	2.4
0502+675	0.314	54 (300)	6e8	<23	1.5e–3	<0.054 (<6e–4)	4	15	3	1	5e4	1e6	0	2.8
0528+134	2.04	420 (1400)	1e9	866	0.13	75 (0.5)	2.6	13	3	1	150	3e3	–1	2.8
0537–441	0.892	216 (360)	2e9	346	0.06	12 (0.04)	3.4	11	3.5	1	90	3e3	0.5	2.2
0650+453	0.933	81 (900)	3e8	212	0.018	4.5 (0.1)	1	15	3	1	90	4.e3	0	2.6
0716+332	0.779	81 (450)	6e8	212	4.5e–3	4.5 (0.05)	4.1	12.2	3	1	150	5e3	0	2.6
0716+714	0.26	84 (700)	4e8	<42	1.5e–3	<0.18 (<3e–3)	1.2	15	3	1	6e3	6e5	1.2	3.2
0735+178	0.424	142 (590)	8e8	<77	3e–3	<0.6 (<5e–3)	0.66	10	3	1	1e3	9.5e3	1	2
0814+425	0.53	30 (500)	2e8	77	2e-3	0.6 (0.02)	3.4	12.9	3	1	100	4e3	1	2.1
	0.53	54 (600)	3e8	<9.5	0.01	<9e-3 (<2e–4)	0.08	14.1	2.5	70	800	4e4	2	2.2
0820+560	1.417	261 (580)	1.5e9	581	0.023	34 (0.15)	3.1	13.9	3	1	220	3e3	0	3.4
0851+202	0.306	90 (600)	5e8	<39	5e–3	<0.15 (<3e–3)	1	10	3	70	2.3e3	6e4	1.2	3.15
0917+449	2.19	900 (500)	6e9	1341	0.1	180 (0.2)	1.95	12.9	3	1	50	4e3	–1	2.6
0948+0022	0.5846	72 (1600)	1.5e8	300	0.024	9 (0.4)	3.4	10	6	1	800	1.6e3	1	2.2
0954+556	0.8955	315 (1050)	1e9	173	7.7e–3	3 (0.02)	0.7	13	2.5	1	6e3	9e3	0.3	2.1
1011+496	0.212	36 (400)	3e8	<12	7e–4	<0.014 (<3e–4)	3.5	15	3	1	6e4	1e5	0.2	3.7
1013+054	1.713	252 (420)	2e9	300	0.036	9 (0.03)	1.7	11.8	3	1	500	3e3	1	2.4
1030+61	1.401	405 (450)	3e9	424	0.022	18 (0.04)	2.1	12.2	3	1	200	7e3	0	3
1050.7+4946	0.140	45 (500)	3e8	<6.7	3e–4	<4.5e–3 (<1e–4)	0.08	17	3	1	2e4	5e6	0.7	3.9
1055+018	0.89	81 (450)	6e8	300	9e–3	9 (0.1)	5.6	12	3	1	30	4e3	1	2.3
1057–79	0.569	99 (550)	6e8	300	5.5e–3	9 (0.1)	4.6	11	3	1	200	4e3	–0.5	3.3
10586+5628	0.143	60 (400)	5e8	<12	1e–3	<0.015 (<2e–4)	0.55	11.5	5	200	1e3	2.8e5	1	2.6
1101+384	0.031	75 (500)	5e8	<0.9	6e–5	<7.5e–5 (<1e–6)	0.25	19	1.8	100	1.3e5	5e5	2	3

Table 4. Input parameters used to model the SED. Sources in italics have been discussed in Paper 1. Note that $R_{\rm BLR}$ is a derived quantity, not an independent input parameter. It is listed for an easy comparison with $R_{\rm diss}$. Col. [1]: name; Col. [2]: redshift; Col. [3]: dissipation radius in units of 10^{15} cm and (in parenthesis) in units of $R_{\rm S}$; Col. [4]: black hole mass in solar masses; Col. [5]: size of the BLR in units of 10^{15} cm; Col. [6]: power injected in the blob calculated in the comoving frame, in units of 10^{45} erg s^{-1}; Col. [7]: accretion disk luminosity in units of 10^{45} erg s^{-1} and (in parenthesis) in units of $L_{\rm Edd}$; Col. [8]: magnetic field in Gauss; Col. [9]: bulk Lorentz factor at $R_{\rm diss}$; Col. [10]: viewing angle in degrees; Col. [11], [12] and [13]: minimum, break and maximum random Lorentz factors of the injected electrons; Col. [14] and [15]: slopes of the injected electron distribution [$Q(\gamma)$] below and above $\gamma_{\rm b}$; For all cases the X–ray corona luminosity $L_X = 0.3 L_{\rm d}$. Its spectral shape is assumed to be $\propto \nu^{-1} \exp(-h\nu/150\ {\rm keV})$.

ton per emitting electron). For the ease of the reader, in these tables we report also the values found and presented in Paper 1.

6.1 Redshifts and black hole masses

The redshift distribution of *Fermi* FSRQs extends to larger values than for BL Lacs (Fig. 1). This has been already pointed out in A09 and is the consequence of BL Lacs being less γ–ray luminous than FSRQs.

The derived black hole masses are in the range (1–60)$\times 10^8 M_\odot$ (Fig. 1). The object for which we could estimate the least massive black hole is PMN 0948+0022, that is a NLSy1 discussed in Abdo et al. (2009b), where a mass of $1.5\times10^8 M_\odot$ was found.

We have searched in the literature other estimates of the black hole masses of our blazars, and report them in Tab. 6. They have been mainly derived from the FWHM of the emission lines, through the assumption of virial velocity of the broad line clouds. There is a rough agreement between our and the other estimates, but note that for specific objects the reported estimates vary by a factor 3–10. It is comforting that the black hole masses assumed here for line–less

Name [1]	z [2]	$R_{\rm diss}$ [3]	M [4]	$R_{\rm BLR}$ [5]	$P'_{\rm i}$ [6]	$L_{\rm d}$ [7]	B [8]	Γ [9]	$\theta_{\rm v}$ [10]	γ_0 [11]	$\gamma_{\rm b}$ [12]	$\gamma_{\rm max}$ [13]	s_1 [14]	s_2 [15]
1127–145	1.184	405 (450)	3e9	1061	0.036	112.5 (0.25)	3.6	12	3	1	150	4e3	0.75	3.3
1144–379	1.049	64.5 (430)	5e8	173	7e-3	3 (0.04)	3.7	12	3	1	300	2e3	1	2.3
1156+295	0.729	114 (380)	1e9	245	0.011	6 (0.04)	4	11.3	3	1	70	5e3	–1	2.8
1215+303	0.13	45 (500)	3e8	<12	4e–4	<0.014 (<3e–4)	0.3	15	3	100	6e3	5e5	1	3.3
1219+285	0.102	75 (500)	5e8	<12	2.3e–4	<0.015 (<2e–4)	0.45	12.9	3	100	2.5e4	6e5	1.7	3.3
1226+023	0.158	120 (500)	8e8	693	0.015	48 (0.4)	11.6	12.9	3	1	40	2e4	1	3.4
1244–255	0.635	71 (340)	7e8	205	5e–3	4.2 (0.04)	4.8	10	3	1	100	4e3	1	2.3
1253–055	0.536	74 (310)	8e8	173	0.012	3 (0.025)	4.5	10.2	3	1	200	3e3	0.5	2.6
1308+32	0.996	115 (550)	7e8	435	0.015	18.9 (0.18)	4.8	13	3	1	300	3e3	1	2.5
1329–049	2.15	450 (1000)	1.5e9	822	0.07	67.5 (0.3)	1.4	15	3	1	300	5e3	1	3.3
1352–104	0.332	23.4 (390)	2e8	77	2.5e–3	0.6 (0.02)	5.5	11.4	3.5	1	50	4e3	0	2.7
1454–354	1.424	150 (250)	2e9	671	0.25	45 (0.15)	2	20.	3	1	1e3	4e3	–1	2.0
1502+106	1.839	450 (500)	3e9	764	0.16	58.5 (0.13)	2.8	12.9	3	1	600	4e3	–1	2.1
1508–055	1.185	360 (600)	2e9	775	9e–3	60 (0.2)	2.7	13	3	1	400	5e3	1	2.9
1510–089	0.360	126 (600)	7e8	205	6e–3	4.2 (0.04)	3.7	14.1	3	1	150	4e3	1	3
1514–231	0.048	105 (700)	5e8	<4.7	2e–3	<2e–3 (<3e–5)	0.4	15	4.3	200	3e3	2e4	2.5	4.6
1520+319	1.487	1500 (2000)	2.5e9	237	0.04	5.6 (0.015)	0.06	15	3	1	2e3	3e4	0.8	2.6
1551+130	1.308	330 (1100)	1e9	755	0.02	57 (0.38)	2	13	3	1	200	6e3	–1	2.4
1553+11	0.36	96 (800)	4e8	<35	7.5e–3	<0.12 (<2e-3)	6	15	3	1	4e4	6e5	0.3	3
1622–253	0.786	360 (300)	4e9	300	0.01	9 (0.015)	1.5	10	3	1	300	6e3	–1	2.6
1633+382	1.814	750 (500)	5e9	866	0.07	75 (0.1)	1.5	12.9	3	1	230	6e3	0	2.9
1652+398	0.0336	63 (300)	7e8	<1.4	1e-4	<2e–4 (<2e–6)	0.11	16	3	200	2e5	2e6	2	3
1717+177	0.137	45 (500)	3e8	<13	1.8e–3	<0.018 (<4e–4)	0.1	12.9	3	100	1e3	1e6	1.8	2.8
1749+096	0.322	172 (820)	7e8	<79	3.5e–3	<0.63 (<6e–3)	1	15	3	1	2e3	1e5	0.9	2.8
1803–784	0.680	66 (440)	5e8	137	6.5e–3	1.88 (0.025)	9.8	12	3	1	20	3.5e3	1	2.2
1846+322	0.798	150 (1000)	5e8	312	6.e–3	9.75 (0.13)	2.5	14	3	1	200	3e3	1	2.5
1849+67	0.657	72 (400)	6e8	212	5.5e–3	4.5 (0.05)	4.6	13	3	1	250	3e3	1	2.3
1908–201	1.119	195 (650)	1e9	548	0.012	30 (0.2)	6.9	14.7	2.4	1	300	2.7e3	1	2.5
1920–211	0.874	150 (500)	1e9	387	8e–3	15 (0.1)	5.2	12.9	3	1	100	5e3	0	2.4
1959+650	0.047	60 (1000)	2e8	<7.7	7e–5	<6e–3 (<2e–4)	1.1	18	3	1	2e5	6e5	1.2	3
2005–489	0.071	83 (550)	5e8	<12	7e–5	<0.015 (<2e–4)	0.9	13.5	3	100	6e4	1e5	1.5	4.3
2023–077	1.388	378 (420)	3e9	474	0.07	22.5 (0.05)	1.8	11.8	3	1	350	4e3	0	2.6
2052–47	1.491	210 (700)	1e9	612	0.045	37.5 (0.25)	2.6	13	3	1	100	7e3	–1	3.0
2141+175	0.213	60 (500)	4e8	268	1.3e–3	7.2 (0.12)	4.3	10	4	1	200	1.5e4	0	3.2
2144+092	1.113	195 (650)	1e9	387	0.02	15 (0.1)	2.4	14.7	3	1	200	5e3	0.5	3.2
2155–304	0.116	72 (300)	8e8	<29	1e–3	<0.084 (<7e–4)	3.5	16	3	1	3e4	2e5	0.5	3.9
	0.116	120 (500)	8e8	<29	3e–4	<0.084 (<7e–4)	0.7	16	3	1	1.8e4	5e5	1	3.3
2155+31	1.486	96 (800)	4e8	110	0.03	1.2 (0.02)	1.2	16	3	1	140	5e3	0.5	3.2
2200+420	0.069	75 (500)	5e8	<17	2.5e–3	<0.03 (<4e–4)	1	10	3	80	150	1e5	1	3.1
2201+171	1.076	180 (300)	2e9	346	0.016	12 (0.04)	5.9	10	3	1	300	3e3	1.2	2.2
2204–54	1.215	195 (650)	1e9	520	0.023	27 (0.18)	3.1	14	3	1	150	3e3	0.5	3.1
2227–088	1.5595	211 (470)	1.5e9	497	0.06	24.8 (0.11)	3.3	12	3	1	200	5e3	0.5	3.2
2230+114	1.037	195 (650)	1e9	670	0.025	45 (0.3)	4.1	14	3	1	110	3e3	0.5	3.1
2251+158	0.859	240 (800)	1e9	548	0.14	30 (0.2)	4.1	13	3	1	250	4e3	1	2.7
2325+093	1.843	420 (1400)	1e9	671	0.08	45 (0.3)	1.6	16	3	1	190	5e3	0	3.5
2345–155	0.621	132 (1100)	4e8	190	3.5e–3	3.6 (0.06)	1.8	13	3	1	100	4e3	–1	2.8
⟨FSRQ⟩	1	189 (630)	1e9	387	0.02	15 (0.1)	2.6	13	3	1	300	3e3	1	2.7
⟨BL Lac⟩	0.1	75.6 (630)	4e8	<24.5	8e–4	<0.06 (<1e–3)	0.8	15	3	1	1.5e4	8.e5	1	3.3

Table 4. – continue –

BL Lacs are consistent with the existing estimates present in the literature.

6.2 Injected power, location of the dissipation region and bulk Lorentz factors

The injected power in relativistic electrons, as measured in the comoving frame, is in the range $P'_{\rm i}=10^{43}$–10^{44} erg s^{-1} for FSRQs and a 10^{41}–10^{43} erg s^{-1} for BL Lacs. Note that we should not compare this power with the power the jet carries in the form of bulk motion of particles and fields, since $P'_{\rm i}$ is measured in the comoving frame. To have comparable quantities, we should multiply $P'_{\rm i}$ by Γ^2.

Among FSRQs, 4 sources have $R_{\rm diss} > R_{\rm BLR}$ (0215+015 and 1520+319, discussed in Paper 1, plus 0954+556 and 1622–253). This means a reduced radiation energy density that in turn implies a weaker radiative cooling and a larger $\gamma_{\rm peak}$. All other

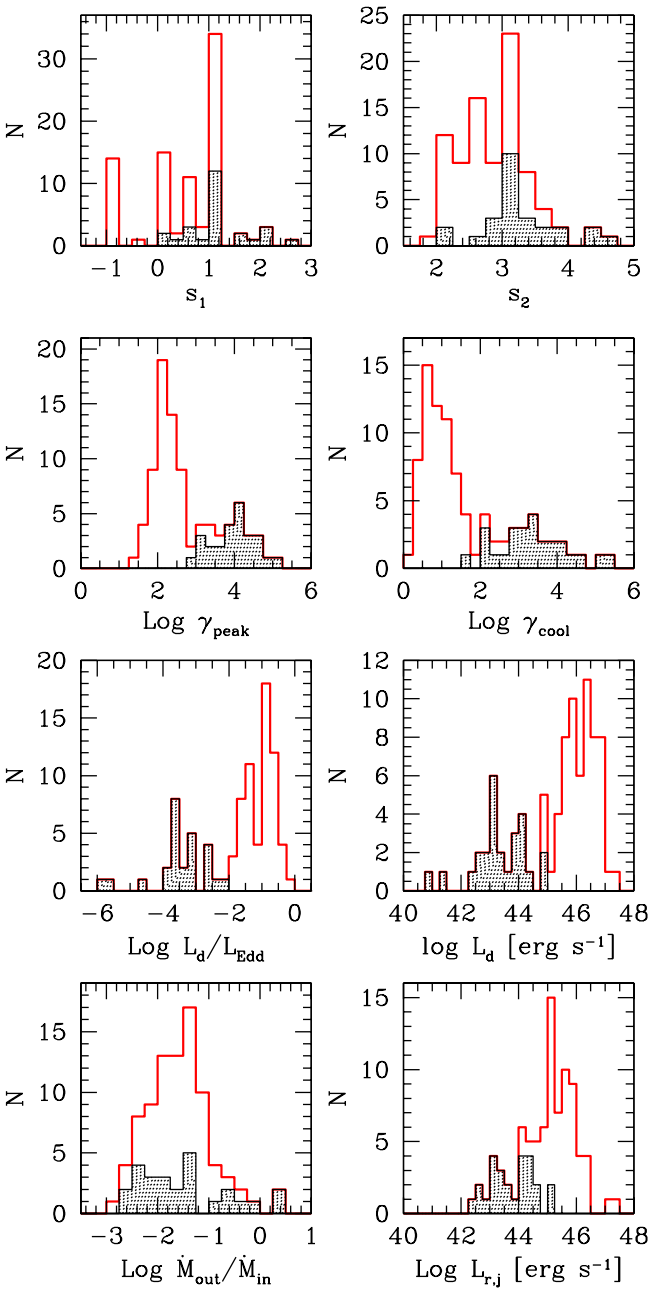

Figure 2. Distributions of the slopes of the injected electron distribution (s_1 and s_2 are the slopes before and after $\gamma_{\rm b}$, respectively), the value of the random Lorentz factor $\gamma_{\rm peak}$ of the electrons radiating at the peaks of the SED, the value of the random Lorentz factor $\gamma_{\rm cool}$ of electrons cooling in one light crossing time $r_{\rm diss}/c$, accretion disk luminosities (also in units of the Eddington one), the ratio between the outflowing and accretion mass rate and the power spent by the jet to produce the radiation we see. Shaded areas correspond to BL Lacs with only an upper limit on their disk accretion luminosity.

FSRQs dissipate within the BLR, at a distance of the order of 300–1000 $R_{\rm S}$ (Fig. 1). For BL Lacs we have the same range of $R_{\rm diss}$.

The distribution of the bulk Lorentz factor is rather narrow, being contained within the 10–15 range, with few BL Lacs having Γ between 15 and 20. The average Γ for BL Lacs is somewhat larger than for FSRQs.

Name	log $P_{\rm r}$	log $P_{\rm B}$	log $P_{\rm e}$	log $P_{\rm p}$
00311–1938	44.37	44.10	43.46	43.93
0048–071	45.75	45.35	44.69	47.10
0116–219	45.16	45.06	44.09	46.26
0118–272	44.20	43.30	43.77	43.91
0133+47	45.22	46.41	44.43	47.01
0142–278	45.39	44.89	44.98	47.26
0202–17	45.80	45.65	44.80	47.31
0208–512	45.44	44.39	44.63	46.44
0215+015	45.81	45.78	44.86	46.09
0218+35	45.21	43.96	44.76	46.51
0219+428	45.16	44.08	44.12	45.44
0227–369	46.18	45.49	44.97	47.34
0235+164	45.78	44.97	44.61	46.60
0301–243	43.66	43.42	43.56	43.93
0332–403	45.41	46.21	44.51	47.05
0347–211	46.30	45.91	44.55	46.92
0426–380	45.48	44.67	44.30	46.36
0447–439	45.41	46.21	44.51	47.05
0454–234	45.60	45.80	44.16	46.40
0502+675	44.53	44.59	42.75	43.29
0528+134	47.39	45.86	45.87	48.31
0537–441	45.80	45.39	44.97	47.19
0650+453	45.55	43.73	44.90	46.88
0716+332	44.77	44.84	44.05	45.92
0716+714	44.36	43.93	44.06	45.21
0735+178	44.19	43.51	44.12	45.12
0814+425 (EC)	44.40	43.81	43.97	45.94
0814+425 (SSC)	44.23	41.35	44.91	45.64
0820+560	45.60	45.75	44.57	46.85
0851+202	44.45	43.48	44.28	44.96
0917+449	46.20	46.29	45.00	47.57
0948+0022	45.30	44.35	44.71	46.68
0954+556	45.04	44.48	44.52	45.07
1011+496	44.19	44.12	42.80	43.21
1013+054	45.68	45.02	44.66	46.99
1030+61	45.50	45.65	44.33	46.62
1050.7+4946	42.53	41.14	43.35	42.81
1055+018	44.93	45.04	44.57	46.90
1057–79	44.75	44.97	44.06	45.85
10586+5628	43.64	42.76	43.72	44.02
1101+384	42.60	42.67	43.03	43.50

Table 5. Jet power in the form of radiation, Poynting flux, bulk motion of electrons and protons (assuming one proton per emitting electron). Sources in italics have been analysed in Paper I and their jet powers are here reported for completeness.

6.3 Magnetic field

On average, we need a slightly larger magnetic field B in FSRQs (1–10 G) than in BL Lacs (0.1–1 G). Note that in our list we lack TeV BL Lacs not detected by *Fermi* (for them, see T09), that have more extreme properties (and smaller magnetic fields) than the sources considered here. Note also that there is one FSRQ with a small magnetic field: this is 1520+319, whose $R_{\rm diss}$ is at very large distances.

6.4 Particle distribution

The average properties of the injected particle distribution can be seen in Fig. 1 and Fig. 2. Note that the *injected* particle distribution $Q(\gamma)$ [cm^{-3} s^{-1}] is different from the *emitting* particle distribu-

Name	$\log P_{\rm r}$	$\log P_{\rm B}$	$\log P_{\rm e}$	$\log P_{\rm p}$
1127–145	45.66	46.06	44.80	47.28
1144–379	44.92	44.49	44.34	46.41
1156+295	45.04	45.12	44.45	46.38
1215+303	43.20	43.46	43.46	42.18
1219+285	43.15	42.92	43.24	43.61
1226+023	45.05	46.09	44.90	47.48
1244–255	44.56	44.64	44.12	46.24
1253–055	45.00	44.71	44.40	46.29
1308+32	45.34	45.28	44.57	46.83
1329–049	46.18	45.53	45.07	47.65
1352–104	44.18	43.94	44.02	45.71
1454–354	47.01	45.13	45.20	47.47
1502+106	46.43	46.12	44.63	46.91
1508–055	45.16	45.78	44.07	46.54
1510–089	44.99	45.26	44.41	46.77
1514–241	43.08	43.17	43.98	44.59
1520+319	45.91	43.84	45.22	46.50
1551+130	45.53	45.45	44.21	46.48
1553+11	45.23	45.44	43.16	44.29
1622–253	44.95	45.04	44.17	45.65
1633+382	46.06	45.91	44.60	47.05
1652+398	42.45	41.66	43.05	43.20
1717+177	43.14	41.23	44.09	44.76
1749+096	44.73	44.40	44.43	45.37
1803+784	44.73	45.35	44.41	46.80
1846+322	45.02	44.99	44.25	46.59
1849+67	44.90	44.83	44.23	46.38
1908–201	45.36	46.18	44.37	46.82
1920–211	45.07	45.58	44.19	46.30
1959+650	43.32	43.72	42.51	43.17
2005–489	42.96	43.66	42.65	43.01
2023–077	45.98	45.41	44.65	46.87
2052–47	45.84	45.27	45.01	47.24
2141+175	44.00	44.39	43.51	45.18
2144+092	45.60	45.25	44.69	46.98
2155–304 (high)	44.40	44.78	43.06	43.85
2155–304 (low)	43.76	43.83	43.40	43.89
2155+31	45.19	43.89	44.98	46.36
2200+420	43.35	43.32	43.94	44.90
2201+171	45.12	45.62	44.36	46.74
2204–54	45.60	45.44	44.80	47.09
2227–088	45.89	45.40	45.07	47.29
2230+114	45.62	45.66	44.89	47.23
2251+158	46.33	45.78	45.43	47.87
2325+093	46.30	45.65	45.06	47.51
2345–1555	44.72	44.56	43.97	45.92

Table 5. – continue –

tion $N(\gamma)$ [cm^{-3}], that is the solution of the continuity equation evaluated at the light crossing time $r_{\rm diss}/c$. It can be seen that the diversity of the blazar spectra requires a rather broad range of s_2, the injected slope for the high energy electrons (between 2 and 4.5), steeper for BL Lac objects. Consider also that when radiative cooling is important (almost always in FSRQs, see the distribution of $\gamma_{\rm cool}$ in Fig. 2), the high energy emitting particle distribution will be characterised by a power law slope s_2+1, i.e. steeper still. The fact that BL Lacs are characterised by a flatter γ–ray spectrum in the *Fermi* band (A09, Ghisellini, Maraschi & Tavecchio 2009) *is not due* to a flatter slope of the $N(\gamma)$ distribution above $\gamma_{\rm b}$, but to their SED peaking at energies close to or higher than a few GeV.

Also the distribution of s_1 is broad, with FSRQs having harder slopes. But in this case the radiative cooling is stronger, and $N(\gamma)\propto\gamma^{-2}$ from $\gamma_{\rm cool}$ to $\gamma_{\rm b}$, making s_1 less important. For BL Lacs, instead, the cooling is much weaker, and in several cases $N(\gamma)\propto\gamma^{-s_1}$ at intermediate energies, mostly contributing to the X–ray band. This requires a softer s_1. There are however extreme cases (TeV emitting BL Lacs, with an hard spectrum) present in T09, but not here (they are not detected by *Fermi*) that require a very hard s_1 or even a cutoff in the electron distribution (i.e. no electrons injected below some critical value).

The distributions of $\gamma_{\rm b}$, $\gamma_{\rm max}$ (Fig. 1) are clearly different for FSRQs and BL Lacs, with BL Lacs requiring much larger values. This, together with the weaker cooling for BL Lacs (implying a larger $\gamma_{\rm cool}$) determines the distribution of $\gamma_{\rm peak}$, the value of Lorentz factors of those electrons producing most of the radiation we see. This confirms earlier results concerning the interpretation of the blazar sequence (i.e. Ghisellini et al. 1998; Celotti & Ghisellini 2008).

The relation of $\gamma_{\rm peak}$ with the energy densities and with $\gamma_{\rm cool}$ is shown in Fig. 3. The top panel shows $\gamma_{\rm peak}$ as a function of the sum of the magnetic and radiation energy density as measured in the comoving frame. The grey symbols are the values for the blazars studied in Celotti & Ghisellini (2008).

6.5 Disk luminosities

The accretion disk luminosities of FSRQs (Fig 2) derived by the model fits are in the range 10^{45}–10^{47} erg s^{-1}, and the upper limits for BL Lacs indicate, always, values below 10^{45} erg s^{-1}. In Eddington units, FSRQs always have values above 10^{-2}, and BL Lacs always values below. Bearing in mind that for some FSRQs our estimates are poor (when the beamed non–thermal flux hide the thermal emission or when *Swift* data are missing) this result is intriguing. It is in perfect agreement with the "blazar's divide" between broad line and line–less objects proposed by Ghisellini, Maraschi & Tavecchio (2009). It also agrees with the scenario proposed by Cavaliere & D'Elia (2002) and Böttcher & Dermer (2002). We will further discuss this point later.

6.6 Accretion and outflow mass rates

Fig. 2 shows the ratio of the accretion ($\dot M_{\rm in}$) and outflow ($\dot M_{\rm out}$) mass rates. For FSRQs we set $\dot M_{\rm out}\equiv P_{\rm j}/(\Gamma c^2)$: therefore $\dot M_{\rm out}$ suffers from the same uncertainties of $P_{\rm j}$, derived assuming one proton per emitting electron and that *all* electrons emit. For completeness we show this distribution also for BL Lacs, but the values are in this case completely uncertain, for two reasons. First, since only an upper limit on $L_{\rm d}$ is derived, we have a corresponding upper limit for $\dot M_{\rm in}$. On the other hand, the disks in BL Lacs may well be radiatively inefficient: if so, they will have larger accretion rates than the ones corresponding to a standard disk. We will estimate $\dot M_{\rm in}$ for BL Lacs later, using the assumption of $P_{\rm j}=\dot M_{\rm in}c^2$.

For FSRQs, instead, the distribution is more meaningful (bearing in mind the limitations mentioned above) and indicates that the mass outflowing rate, on average, is 1–10% of the mass accretion rate. The distribution is rather narrow, and this may indicate that the mass outflow rate of the jet (derived assuming one proton per emitting electron) is linked with the mass accretion rate. In other words, the matter of the jet may come directly from the accreting one, with other process, like entrainment, less important.

Name			Ref		Ref		Ref
0502+675	8.78	8.80	F03b				
0851+202	8.7	8.79	W04				
1011+496	8.48	8.71	F03b	8.28	W08	8.32	W02
		8.25	W02	8.25	W02		
1101+384	8.7	8.29	W08	8.42	W08	8.97	W08
		9.13	W02	8.88	W02		
1215+303	8.48	8.83	F03b	7.53	W02	7.62	W02
1514–241	8.7	8.74	F03a	8.09	B03	8.74	F03b
		8.40	Wo05	9.10	W02	8.86	W02
1652+398	8.84	9.21	W08	8.78	W08	8.62	Wo05
		8.94	F03	9.21	B03		
1749+096	8.84	8.66	F03b	7.21	W02	7.36	W02
1959+650	8.3	8.08	W08	8.28	W08	7.96	Wo05
		8.56	F03a	8.30	W02	8.22	W02
		8.53	F03b				
2005–489	8.7	8.14	W08	8.89	F03b	8.66	W02
		8.51	W02				
2200+420	8.7	8.08	W08	8.28	W08	8.35	W04
		8.77	F03b	8.56	W02	8.43	W02
0537–441	9.3	8.74	W04	7.7	P05	8.33	L06
0820+560	9.18	9.49	C09				
0917+449	9.78	9.88	C09				
0948+002	8.17	8.26	C09				
0954+566	9	9.20	C09	7.7	P05	7.87	L06
1013+054	9.3	9.78	C09				
1030+61	9.48	9.39	C09				
1055+018	8.78	9.25	C09				
1144–379	8.7	7.6	P05				
1156+295	9	9.11	C09	8.56	X05	8.54	X05
		8.63	P05	8.54	L06		
1226+023	8.9	9.10	F03b	9.21	W04	8.6	P05
		8.92	L06				
1253–055	8.9	8.48	W04	7.9	P05	8.28	L06
1308+32	8.84	8.94	C09	9.24	W04		
1502+106	9.48	9.50	C09	8.74	L06		
1510–089	8.84	8.62	W04	8.31	X05		
		8.22	X05	8.20	L06		
1551+130	9	9.19	C09				
1633+382	9.7	9.74	C09	8.67	L06		
1803+784	8.7	8.57	W04	7.92	L06		
2141+175	8.6	8.98	F03b	8.14	X05	8.05	X05
		7.95	L06				
2227–088	9.18	9.40	C09				
2230+114	9	8.5	P05				
2251+158	9	9.10	W04	8.5	P05	8.83	L06

Table 6. Estimates of the mass of the black hole for the blazars in our sample. Values are given for the logarithm of the black hole mass measured in solar masses. We list here only those blazars for which we have found another, independent, mass estimate. The first value (Col. 2) is the estimate found in this paper. In the top part of the table we list BL Lacs for which we found only an upper limit on the disk luminosity. In this case our estimates of the black hole mass is very uncertain. References: B03: Barth et al. (2003); C09: cheng et al. (2009); F03a: Falomo et al. (2003a); F03b: Falomo et al. (2003a); L06: Liu et al. (2006); P05: Pian et al. (2005); W02: Wu et al. (2002); W04: Wang et al. (2004); W08: Wagner (2008); Wo05: Woo et al. (2005). X05: Wie et al. (2005);

6.7 Emission mechanisms

For all but four FSRQs (0215+015, 0954+556, 1520+319 and 1622–253) the dissipation region is within the BLR, that provides most of the seed photons scattered at high frequencies. The main emission processes are then synchrotron and thermal emission from the accretion disk for the low frequency parts, and External Compton for the hard X–rays and the γ–ray part of the spectrum. The X–ray corona and the SSC flux marginally contribute to the soft X–ray part of the SED. When $R_{\rm diss} < R_{\rm BLR}$ the overall non–thermal emission is rather insensitive to the presence/absence of the IR torus, since the bulk of the seed photons are provided by the broad lines. Instead, for the 4 FSRQs with $R_{\rm diss} > R_{\rm BLR}$, the external Compton process with the IR radiation of the torus is crucial to explain their SED.

For BL Lacs (see the SEDs in T09) the main mechanism is SSC, but in few cases this process is unable to account for a very large separation between the synchrotron and the inverse Compton peaks of the SED, without invoking extremely large bulk Lorentz factors (larger than 100). These are the cases where the SED is better modelled invoking an extra source of seed photons for the IC process, besides the ones produced by synchrotron in the same zone. One possibility is offered by the spine/layer scenario (Ghisellini, Tavecchio & Chiaberge 2005), in which a slower layer surrounds the fast spine of the jet. The radiative interplay between the two structures enhances the IC flux and can account for the observed SED in these cases.

Another problem, with the standard one–zone SSC scenario, concerns the ultrafast (i.e. minutes) variability sometimes seen at high energies (Aharonian et al. 2007, Albert et al. 2007). This cannot be accounted for by the simple models, and require other emitting zones or extra population of electrons (see e.g. Ghisellini & Tavecchio 2008; Ghisellini et al. 2009b; Giannios, Uzdensky & Begelman 2009).

For all our sources the importance of the γ–$\gamma \to e^{\pm}$ process (which is included in our model) is very modest, and does not influence the observed spectrum, nor the derived jet power, discussed below.

7 JET POWER

Table 5 lists the power carried by the jet in the form of radiation ($P_{\rm r}$), magnetic field ($P_{\rm B}$), electrons ($P_{\rm e}$) and cold protons ($P_{\rm p}$, assuming one proton per emitting electron). All the powers are calculated as

$$P_i \, = \, \pi r_{\rm diss}^2 \Gamma^2 \beta c \, U_i' \qquad (3)$$

where U_i' is the energy density of the i component, as measured in the comoving frame. We comment below on each contribution:

- The power carried in the form of the produced radiation, $P_{\rm r} \, = \, \pi r_{\rm diss}^2 \Gamma^2 \beta c \, U_{\rm rad}'$, can be re–written as [using $U_{\rm rad}' \, = \, L'/(4\pi r_{\rm diss}^2 c)$]:

$$P_{\rm r} \, = \, L' \frac{\Gamma^2}{4} \, = \, L \frac{\Gamma^2}{4\delta^4} \, \sim \, L \frac{1}{4\delta^2} \qquad (4)$$

where L is the total observed non–thermal luminosity (L' is in the comoving frame) and $U_{\rm rad}'$ is the radiation energy density produced by the jet (i.e. excluding the external components). The last equality assumes $\theta_{\rm v} \, \sim \, 1/\Gamma$. This is a almost model–independent quantity, since it depends only on the adopted δ, that can be estimated also by other means, namely superluminal motions.

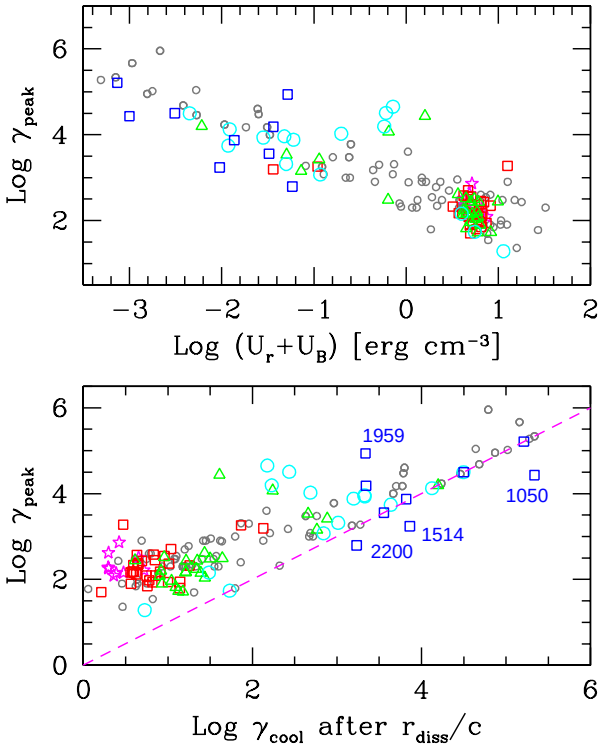

Figure 3. Top: $\gamma_{\rm peak}$ vs $U_B + U'_{\rm r}$. Bottom: $\gamma_{\rm peak}$ vs $\gamma_{\rm cool}$ calculated after one light crossing time. The dashed line indicates equality. See text for details. Different symbols refer to different γ–ray luminosity bins, as in Fig 6. For comparison, we show (little grey circles) the blazars studied in Celotti & Ghisellini (2008).

• When calculating $P_{\rm e}$ (the jet power in bulk motion of emitting electrons) we include their average energy, i.e. $U'_{\rm e} = n_{\rm e}\langle\gamma\rangle m_{\rm e}c^2$. Usually, when estimating this quantity, we have the problem of determining $\gamma_{\rm min}m_{\rm e}c^2$, the minimum energy of the electron distribution [where, for steep distribution functions $N(\gamma)$, most of the electrons are]. This problem is much alleviated here, since the assumed form of the particle injection function $Q(\gamma)$ is rather flat at low energies. The amount of the electrons at low energies then mainly depends on cooling, making $N(\gamma) \propto \gamma^{-2}$ down to $\gamma_{\rm cool}$, and flatter below. Thus the total amount of electrons contributing to $P_{\rm e}$ depends on cooling, not on a pre–assigned shape of the particle distribution (including a pre–assigned $\gamma_{\rm min}$). In this sense the $P_{\rm e}$ derived here is less arbitrary. Furthermore, in the case of luminous FSRQs, the X–ray flux can be reliably associated to the EC mechanism (this occurs when the slope is very hard, because the SSC component tends to be rather softer, see the discussion of this point in Celotti & Ghisellini 2008). In this case the low energy X–ray data are crucial to fix $\gamma_{\rm min}$: a too high value makes the modelled X–ray flux to underestimate the observed one. Since in this sources the radiative cooling is severe, this agrees with the fact that $\gamma_{\rm min}$ must be small, of the order of $\gamma_{\rm cool}$ or less. As a final comment, consider that the estimate of $P_{\rm e}$ includes only those electrons contributing to the emission. Since it is unlikely that all the electrons present in the emitting region are accelerated, $P_{\rm e}$ is a lower limit. On the other hand, when $\langle\gamma\rangle$ is greater than a few, the contribution of the accelerated electrons to $P_{\rm e}$ may dominate over the contribution of the cool (not accelerated) ones.

• For $P_{\rm p}$ (the jet power in bulk motion of cold protons) we have assumed that there is one proton per emitting electron, i.e. electron–positron pairs are negligible. This is a crucial assumption. Partly, it is justified within the context of our model because we take into account the pair production process, and we find that pairs are always negligible. If a substantial amount of pairs comes from the inner regions of the jet we must explain why they have survived annihilation, important in the inner, more compact and denser regions (Ghisellini et al. 1992). If they have survived because they were hot (thus they had a smaller annihilation cross section) then they should have produced a large amount of radiation (that we do not observe). In doing so, they should have cooled rapidly, and then annihilate. These considerations (see also similar comments in Celotti & Ghisellini 2008) lead us to accept the assumption of one proton per electron as the most reliable.

For BL Lacs the presence or not of electron–positron pairs is less of a problem, because the mean energy of the emitting electrons is large, approaching the rest mass–energy of a proton. In this cases $P_{\rm e} \sim P_{\rm p}$.

• $P_{\rm B}$ is derived using the magnetic field found from the model fitting. There can be the (somewhat contrived) possibility that the size of the emitting region is smaller than the one considered here, i.e. inside the jet there could be smaller volumes where the magnetic field lines reconnect, and in this case the total Poynting flux of the jet can be larger than what we estimate here. We consider that this is unlikely.

Fig. 4 shows the distributions of the jet powers and the bottom panel, for comparison, shows the distribution of the accretion disk luminosities. Grey shaded ares correspond to BL Lacs for which we could estimate only an upper limit to their disk luminosity. Fig. 5 shows the fraction of the total jet power (i.e. $P_{\rm p} + P_{\rm e} + P_{\rm B}$) transformed in radiation ($\epsilon_{\rm r}$), carried by electrons ($\epsilon_{\rm e}$) and Poynting flux ($\epsilon_{\rm B}$).

For FSRQs the power carried in radiation ($P_{\rm r}$) is larger than $P_{\rm e}$. This is a consequence of fast cooling: electrons convert their energy into radiation in a time shorter than $r_{\rm diss}/c$ and the radiation component can in this time accumulate more energy than what remains in the electrons (even if they are continuously injected during this time). The distribution of $P_{\rm B}$ is at slightly smaller values than the distribution of $P_{\rm r}$, indicating that the Poynting flux cannot be at the origin of the radiation we see. As described in Celotti & Ghisellini (2008), this is a direct consequence of the large values of the so called Compton dominance (i.e. the ratio of the Compton to the synchrotron luminosity), since this limits the value of the magnetic field.

To justify the power that the jet carries in radiation (we insist: it is the least controversial quantity) we are forced to consider the power carried by the jet in the form of protons. Following the consideration made above, the simplest and most reasonable assumption is to assume that there is one proton per electrons. If so, $P_{\rm p}$ for FSRQs is a factor $\sim$10–100 larger than $P_{\rm r}$, meaning an efficiency of 1–10% for the jet to convert its bulk kinetic motion into radiation (see also the top panel of Fig. 5). This is reasonable: most of the jet power in FSRQs goes to form and energise the large radio structures, and not into radiation. On the other hand, we do not have yet a firm handle on how much power the radio–lobes require (this estimate, among other things, depends on the proton energy density, still a very poorly known quantity). Another inference comes from blazars emitting X–rays at large ($\sim$10–100 kpc) distances as observed by Chandra. For them the leading emission model (e.g. Tavecchio et al. 2004, 2007; but see. e.g., Kataoka et al. 2008) requires that the jet is still relativistic at those scales (with Γ–factors similar to the ones derived in the inner regions) and this in turn

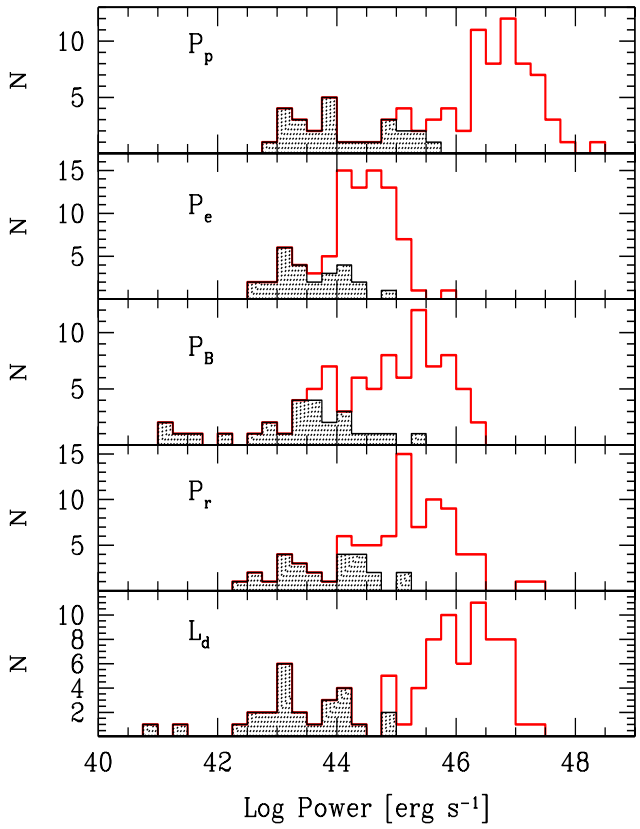

Figure 4. From top to bottom: distributions of the jet power in the form of bulk kinetic power of cold protons ($P_{\rm p}$, assuming one proton per emitting electron); emitting electrons ($P_{\rm e}$, including their average random energy $\langle\gamma\rangle m_{\rm e}c^2$); Poynting flux ($P_{\rm B}$), radiation ($P_{\rm r}$). The bottom panel shows the distribution of the luminosities $L_{\rm d}$ of the accretion disk. The shaded area in all panels corresponds to sources with only upper limits on $L_{\rm d}$.

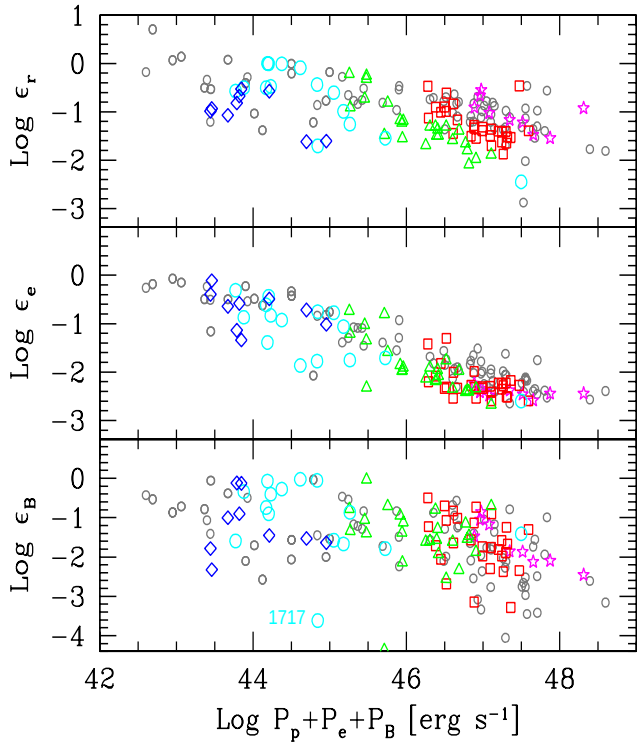

Figure 5. The fraction of $L_{\rm jet}$ radiated ($\epsilon_{\rm r}$, top panel), in relativistic leptons ($\epsilon_{\rm e}$, mid panel) and in magnetic fields (ϵ_B, bottom panel) as functions of $P_{\rm jet} = P{\rm p} + P_{\rm e} + P_{\rm B}$. Different symbols refer to different γ–ray luminosity bins, as in Fig 6. For comparison, we show (little grey circles) the blazars studied in Celotti & Ghisellini (2008).

suggests that the jet has not lost much of its power in producing radiation.

Consider now BL Lacs: we still have that $P_{\rm r} \sim P_{\rm e} \gtrsim P_{\rm B}$, but now also $P_{\rm p}$ is of the same order. This means that we are using virtually all the available jet power to produce the radiation we see. This is also illustrated in Fig. 5. Thus for BL Lacs we either assume that not all electrons are accelerated, allowing for an extra reservoir of power in bulk motion of the protons, or, more intriguingly, we conclude *that the jet noticeably decelerates*. The latter option is in agreement with recent findings on the absence of fast superluminal motion in TeV BL Lacs (Piner & Edward 2004; Piner, Pant & Edwards 2008), with the absence of strong extended radio structures, and with the result of the *Chandra* observations of extended X–ray jets at large scales, showing sub-luminal speed at large scales (e.g. Worrall et al. 2001; Kataoka & Stawarz 2005). Moreover, this issue of jet deceleration of BL Lac jets has been debated recently on the theoretical point of view (Georganopoulos & Kazanas 2003; Ghisellini, Tavecchio & Chiaberge 2005).

We conclude that the jet of FSRQs are powerful, matter dominated and transforming a few per cent of their kinetic power into radiation. The jet of BL Lacs are less powerful, with the different forms of power in rough equipartition, transforming a larger fraction of their kinetic power into radiation, and probably decelerating. Despite these different characteristics, there is no discontinuity between FSRQs and BL Lacs. All the different properties can be explained with the difference in jet power accompanied by a different environment, in turn caused by a different regime of accretion. This important point is discussed below.

7.1 Jet power vs accretion luminosity

The availability of the *Swift*/UVOT data for many of our blazars made possible to estimate the accretion disk luminosity for several of them. We can then discuss one of the crucial problem in jet physics: the disk/jet connection.

Fig. 6 shows what we think is the main result of our work (see also Maraschi & Tavecchio 2003, Sambruna et al. 2006 for earlier results). The top panel shows $P_{\rm r}$ as a function of the accretion disk luminosity $L_{\rm d}$, while the bottom panel shows $P_{\rm jet}$ vs $L_{\rm d}$. The different symbols correspond to different bins of the observed γ–ray luminosity L_γ, as labelled.

Consider first the top panel:

- Blazars with different L_γ form a sequence in the $P_{\rm r}$–$L_{\rm d}$ plane. That L_γ correlates with $P_{\rm r}$ is not a surprise, since we already knew (from EGRET) that the γ–ray luminosity is dominating the bolometric output. What is interesting is that the most luminous γ–ray blazars have also a more powerful accretion disk.
- For our analysis we have considered the average value of the γ–ray luminosity during the 3 months survey. Then it should not be extreme, given the large amplitude and rapid variability shown by blazars, especially at high energies. In other words, the shown $P_{\rm r}$ is more indicative of an "average" state, not of an extremely high state, even if, in a flux limited sample of variable sources, like

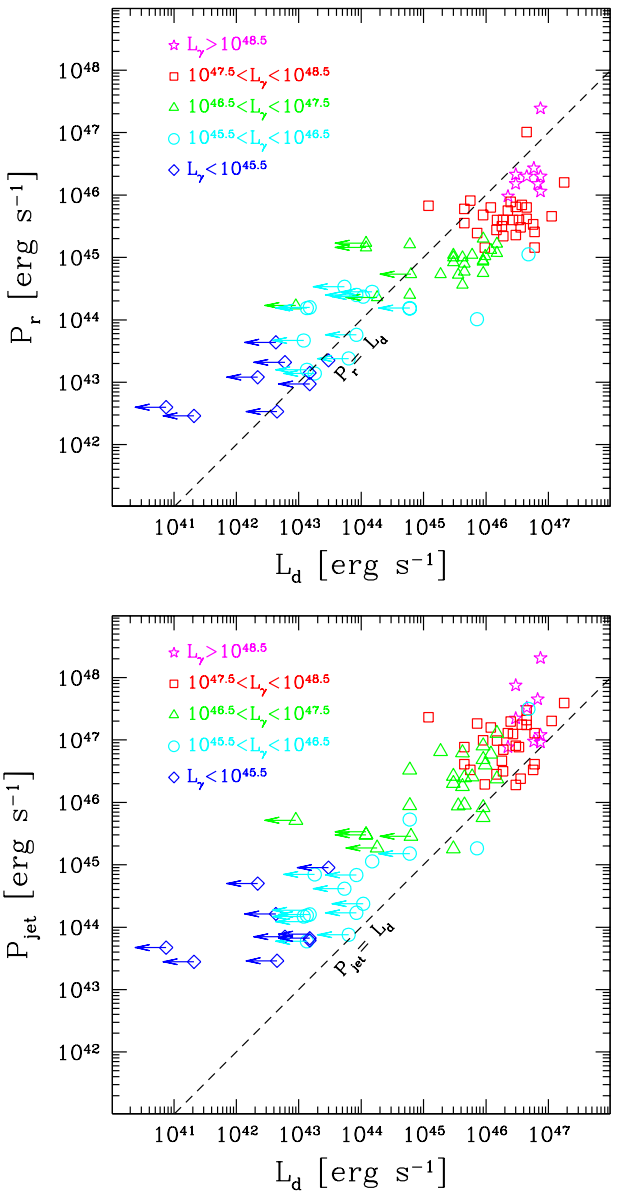

Figure 6. Top: The radiation power produced by the jet as a function of the accretion disk luminosity. Bottom panel: the jet power (i.e. $P_{\rm jet} = P_{\rm p} + P_{\rm e} + P_{\rm B}$) as a function of the accretion disk luminosity. The different symbols (as labelled) correspond to blazars of different γ–ray observed luminosities.

the *Fermi* one, sources in high states are always over–represented. Variability of $P_{\rm r}$ is however an issue, and we can consider that the single blazar can vary at least by a factor 10–30 around the shown $P_{\rm r}$. This contributes to the somewhat large scatter around the $P_{\rm r}$–$L_{\rm d}$ relation.

- Considering only FSRQs, we have that a least square fit yields $\log P_{\rm r,45} = 0.73 \log L_{\rm d,45} - 0.36$, with a probability for the correlation to be random of $P = 5 \times 10^{-8}$. The same least square fit yields $\log L_{\rm d,45} = 0.65 \log P_{\rm r,45} + 0.82$, indicating that a slope around unity is consistent with the data. Since both $P_{\rm r}$ and $L_{\rm d}$ depends on redshift, we have also applied a partial correlation analysis, as explained in Padovani (1992). Using Eq. 1 of that paper, we have verified that $P_{\rm r}$ and $L_{\rm d}$, once the redshift dependence is excluded, still correlate, although the probability to be random increases to $P = 2 \times 10^{-4}$.
- Line–less BL Lacs are shown with their corresponding upper limits on $L_{\rm d}$. These are nevertheless important, showing that they must deviate from the general trend defined by FSRQs (see also Maraschi & Tavecchio 2003).

Consider now the bottom panel, showing $P_{\rm jet}$ vs $L_{\rm d}$. As mentioned, the jet power of FSRQs is dominated by the bulk motion of cold protons, while in BL Lacs it is more equally distributed among electrons, protons and magnetic field. Also in this plane the more γ–ray luminous blazars have the most powerful jet.

Considering only FSRQs, we have that a least square fit yields $\log P_{\rm jet,45} = 0.62 \log L_{\rm d,45} + 1.07$, with a probability for the correlation to be random of $P = 6 \times 10^{-7}$. The same least square fit yields $\log L_{\rm d,45} = 0.56 \log P_{\rm jet,45} + 0.14$, indicating that a slope around unity is consistent with the data. Excluding the dependence of redshift by applying a partial correlation analysis, the probability to be random increases to $P = 3.4 \times 10^{-6}$.

Also in this plane the line–less BL Lacs (with upper limits for $L_{\rm d}$) deviate from the trend defined by FSRQs, implying that their jet is much more powerful than the luminosity emitted by their accretion disks.

We now assume, as an ansatz, that the jet power is always of the order of $\dot M_{\rm in} c^2$, for FSRQ as well as for BL Lacs (see Ghisellini & Tavecchio 2008 for a discussion). This allows to estimate the accretion rate for BL Lacs independently from their (invisible) disk luminosity. Furthermore we can form the ratio $\dot M_{\rm in}/\dot M_{\rm Edd}$ given by

$$\frac{\dot M_{\rm in}}{\dot M_{\rm Edd}} \equiv \frac{\dot M_{\rm in} c^2}{1.3 \times 10^{38} (M/M_\odot)} \qquad (5)$$

For FSRQs we have used $\dot M_{\rm in}$ and M derived from our modelling ($\dot M_{\rm in}$ is given by $\dot M_{\rm in} = L_{\rm d}/(\eta c^2)$, with $\eta = 0.08$ for all sources). For BL Lacs we simply set $\dot M_{\rm in} = P_{\rm jet}/c^2$. The resulting distributions are shown in Fig. 7. Since for BL Lacs the mass we have used is very uncertain, although in agreement with other independent estimates, we show, beside the values of $\dot M_{\rm in}/\dot M_{\rm Edd}$ obtained using the masses listed in Tab. 4 (thick solid line), also the distribution obtained by adopting the same mass of 10^8 (shaded cyan) and $10^9 M_\odot$ (shaded gray) for all BL Lacs.

Fig. 7 shows that there is a "divide" between BL Lacs and FSRQs occurring at $\dot M_{\rm in}/\dot M_{\rm Edd} \sim 0.1$, equivalent to $L_{\rm d}/L_{\rm Edd} \sim 0.01$, in striking agreement with the value proposed by Ghisellini, Maraschi & Tavecchio (2009) and very similar to the value proposed by Ghisellini & Celotti (2001) for the division between FR 1 and FR 2 radio–galaxies, based on completely different arguments (see also Xu, Cao & Wu 2009). This division can be readily interpreted as the change in the accretion regime of the disk, becoming radiatively inefficient when $\dot M_{\rm in}$ is less than $\sim 10\%$ of the Eddington value (and $L_{\rm d}$ is less than $\sim 1\%$ of $L_{\rm Edd}$). Notably, there are hints that similar results holds for *radio-quiet* sources (e.g. Ho 2009; see also Ho 2008 for review).

8 SUMMARY OF RESULTS

We have studied the entire sample of blazars detected during the first 3–months survey of *Fermi* and have a known redshift and a reasonable data coverage of their SED. By studying the resulting 85 objects we have found the following main results:

- The simultaneous or quasi–simultaneous *Swift* observations

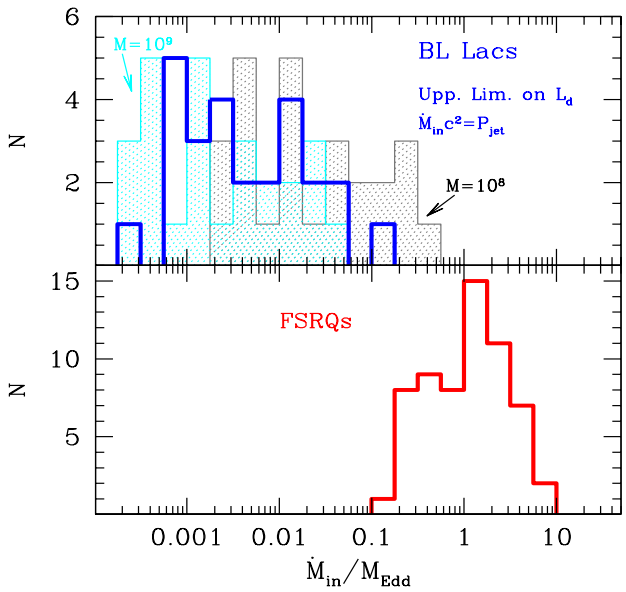

Figure 7. Distributions of the accretion rates in Eddington units for BL Lacs, calculated assuming $P_{\rm j} = \dot{M}_{\rm in}c^2$ (top panel) and for FSRQs (bottom). The assumed black hole mass is listed in Tab. 4. For BL Lacs, given the uncertain estimates of the mass, we also report two other distributions, assuming a mass of $M = 10^8\,M_\odot$ and $M = 10^9\,M_\odot$ (grey and cyan histograms, respectively) for all the sources.

for a large fraction of our sources allowed to have an unprecedented view on the optical to γ–ray SED of blazars. In addition, the optical–UV data were very important to separate the thermal emission produced by the accretion disk from the beamed non–thermal continuum. In this way, for FSRQs, we could estimate the black hole mass and the accretion rate. This in turn allowed to study the connection between the power of the jet and the luminosity emitted by the accretion disk. We found that they correlate.

- The estimated black hole masses are in the range between 10^8 and several times 10^9 solar masses for FSRQs. For BL Lacs the poorly constrained masses are in the range $10^8 - 10^9 M_\odot$. These values are consistent with those found in the literature for the same objects, but existing estimates vary.
- The luminosity emitted by the accretion disks of FSRQs is between 1 and 60 per cent of the Eddington one. Upper limits to the disk emission of BL Lacs indicate $L_{\rm d}/L_{\rm Edd} < 10^{-2}$.
- The "divide" between FSRQs and BL Lacs, in terms of the accreting mass rate (Ghisellini, Maraschi & Tavecchio 2009), is fully confirmed. It occurs when the accretion mass rate becomes smaller than 10 per cent of the Eddington one, or, equivalently, when the disk luminosity becomes smaller than 1 per cent Eddington.
- The γ–ray luminosity is a good tracer both of the accretion disk luminosity (for FSRQs) and of the jet power (for all blazars).
- As for the jet emission processes, the EC component almost always dominates the emission beyond the X–ray band in FSRQs, with the SSC contributing to soft and mid–energy X–rays in some cases. In BL Lacs, most of the sources can be fitted by a pure SSC model, but some of them require an extra component when the separation, in energy, of the synchrotron and Compton peaks is too large. This can be provided by a spine/layer structure of the jet, that avoids the need of extremely large Γ–factors.
- The seed photons for the EC mechanism can be provided by a fairly standard BLR, as assumed here and in the "canonical" scenario for powerful blazars. The majority of FSRQs dissipate within the BLR, while 4 of them are better fitted assuming a dissipation region between the BLR and an IR emitting torus, at distances greater than the BLR.
- The jet dissipation region is located between a few hundred and a thousand Schwarzschild radii for all sources.
- Bulk Lorentz factors are in the range 10–15.
- The magnetic field in the emitting region of FSRQs is between 1 and 10 G, and 10 times less for BL Lacs, on average.
- Jets in FSRQs must be matter dominated, while in BL Lacs there can be equipartition between the power in bulk motion of the emitting electrons, cold protons and magnetic field.
- In FSRQs it is likely that the electron-positron pair component is negligible. If so, the jet power in these sources is dominated (by a factor 10–30) by the cold proton component, and it is a factor $\sim$3–5 larger than the luminosity emitted by the accretion disk. The outflowing mass rate is around a few per cent of the accreting mass rate.
- We confirm that the SEDs of blazar form a sequence, explained in terms of different radiative cooling suffered by the electrons, with higher energy electrons present in jets of lower power.

9 DISCUSSION

The results listed in the previous section confirm earlier findings, largely based on blazars with an EGRET detection, and/or detections in the TeV band. Because of the factor ~ 20 better sensitivity of *Fermi*/LAT with respect to EGRET, we are now starting to explore sources that are not in "extraordinary" bright states in γ–ray band. Sources in our sample should be closer to the average state of blazars, even if, given the still limited sensitivity and the large amplitude variability (even by factor 30–100) our blazars are most likely emitting above their average.

These *Fermi* blazars confirm that the jet of blazars form a sequence whose main parameter is their emitted luminosity. This may seem strange, given the strong dependence of the observed luminosity to the Doppler beaming, then on the viewing angle. On the other hand, the results of our model fitting show that our blazars are all viewed at small angles, with no misaligned jet entering the sample. Misaligned sources, therefore, are fainter than the current *Fermi* blazars and should appear in deeper catalogues.

9.1 Black hole mass and the blazar sequence

There is, in our opinion (Ghisellini & Tavecchio 2008), another important parameter, besides the jet power, controlling the look of the emitted SED and its bolometric luminosity: the mass of the black hole. Blazars with small black hole masses and accreting at a rate greater than a critical value should be "red" (i.e. they should have relatively small peak frequencies and large Compton dominance) even if their observed bolometric luminosity is relatively small, contrary to what the simplest version of the blazar sequence would predict. Fig. 8 shows the observed bolometric luminosity (as derived by the model) as a function of the black hole mass estimated in this paper. Empty circles are FSRQs with estimated black hole masses and accretion luminosities, filled circles are BL Lacs with only an upper limit on their disk luminosities, and whose black hole mass is uncertain. We also show the range of black hole masses existing in the literature and reported in Tab. 6. Within FSRQs there is indeed a tendency for larger luminosities to correspond to larger black hole masses. Viceversa, below $L_{\rm obs} = 10^{47}$ erg s^{-1} all black

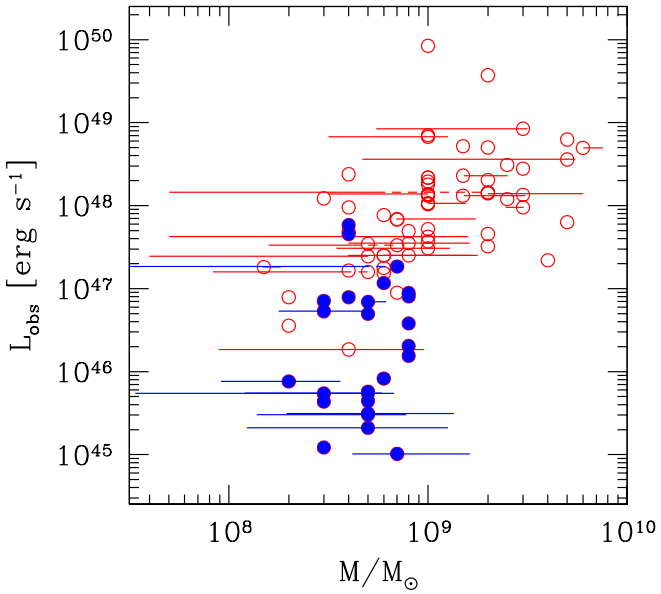

Figure 8. The observed bolometric luminosity produced by the jet (calculated from the fitting model) as a function of the black hole mass. Empty circles are FSRQs with estimated black hole masses and accretion luminosities, filled circles are BL Lacs with only an upper limit on their disk luminosities, and whose black hole mass is uncertain. We also show the range of the estimates of the black hole mass found in the literature.

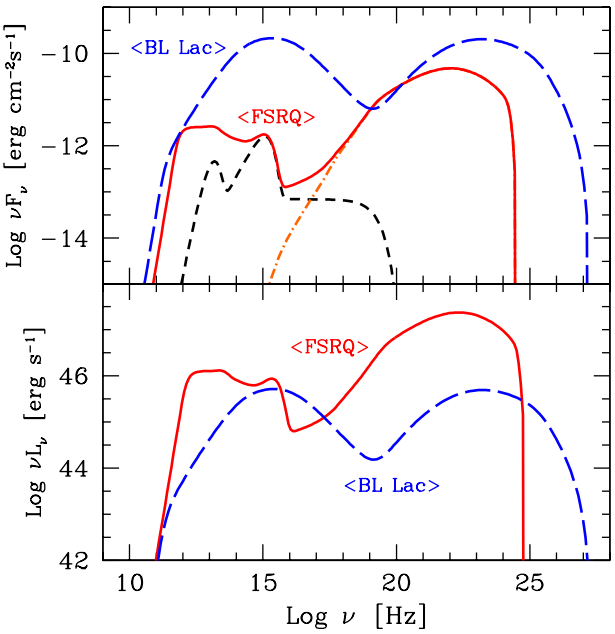

Figure 9. The average SED of FSRQs and of BL Lacs without any sign of disc emission. These SED have been constructed taking the (logarithmic) average of the parameters of the sources belonging to the two subclasses (see Table 4). The top and the bottom panels show the fluxes and luminosities, respectively. The shown frequencies are calculated in the rest frame of the source for the luminosity plot, and are the observed ones for the flux plot. The assumed redshift are $z = 1$ for $\langle$FSRQ$\rangle$ and $z = 0.1$ for $\langle$BL Lac$\rangle$.

hole masses are smaller than $10^9 M_\odot$. Fig. 8 shows that there can be "red" blazars with $L_{\rm obs}$ similar to (bluer) BL Lacs, but this happens when their black hole mass is relatively small.

Having the distribution of all relevant physical parameters, we can do the exercise to construct the "average" SED of FSRQs and BL Lacs, respectively, of our sample. This is illustrated by Fig. 9, for which we have used for the average FSRQs and BL Lacs the parameters listed at the end of Tab. 4. Note that in our sample there are no "extreme" TeV BL Lacs, since, as discussed in T09, these sources have so large Compton peak frequencies to make difficult a detection by *Fermi*. So Fig. 9 corresponds to the average BL Lac detected by *Fermi*, and not to the average BL Lac in general.

9.2 Jet power and accretion

The jet powers derived here are large, reaching, at the high end of their distributions, values greater than 10 times the disk luminosity (see the upper panel of Fig. 10). For these extreme objects $P_{\rm jet} \gtrsim \dot{M}_{\rm in} c^2$. This is admittedly a model–dependent statement. It assumes a one–zone leptonic model and that there is one proton per emitting electron. A more robust statement is that the amount of power the jet spends to produce and carry the non–thermal radiation is also very large, being in some case equal to the disk luminosity produced by accretion (see the bottom panel of Fig. 10), and more often a factor ∼3–10 smaller. Consider that the jet power cannot be simply be represented by $P_{\rm r}$: if this were the case, the entire jet power is used to produce the radiation we see, so that the jet would decelerate significantly. Instead, the jet *must* continue to be relativistic up to large distances, as required by the existence of strong radio lobes and the X–ray radiation seen by the *Chandra* satellite at distances (from the black hole) of hundreds of kpc. Therefore a reasonable *lower limit* on $P_{\rm jet}$ should be a factor 3–10 greater than $P_{\rm r}$.

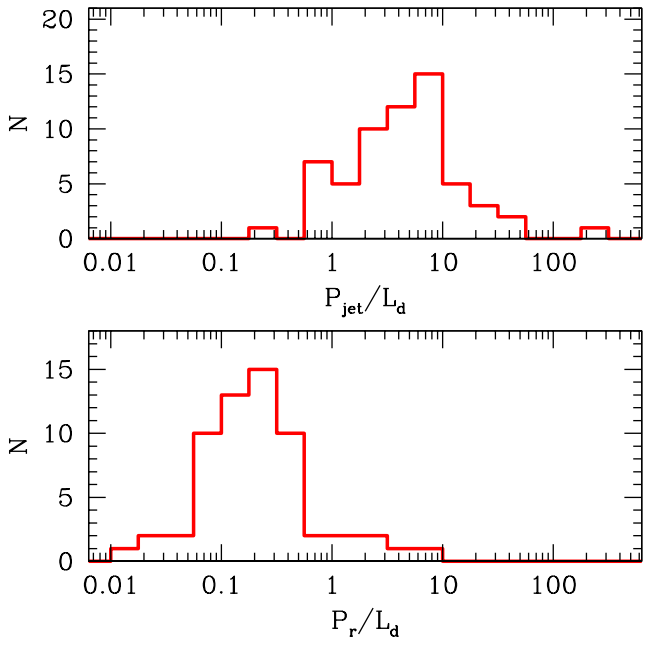

Figure 10. Top panel: the distribution of the ratio between the total jet power $P_{\rm jet}$ and the accretion disk luminosity $L_{\rm d}$. Bottom panel: The distribution of the ratio between $P_{\rm r}$ (the power carried by the jet in the form of produced radiation) and the accretion disk luminosity $L_{\rm d}$. Both distributions are for FSRQs only.

What is then the source of the power of the jet? Is it only the gravitational energy of the accreting matter or do we necessarily need also the rotational energy of a spinning black hole? We here discuss two possible alternatives, that can both explain our results, but are drastically different for the ultimate energy source for the jet.

Jets powered by accretion only — Jolley et al. (2009), building up on previous ideas put forward in Jolley & Kuncic (2008), propose that, in jetted sources, a sizeable fraction of the accretion power goes to power the jet. As a result, the remaining power for the disk luminosity is less than usually estimated by setting $L_{\rm d} = \eta \dot{M}_{\rm in} c^2$, with $\eta \sim 0.08$–0.1. This implies that the mass accretion rate needed to sustain a given $L_{\rm d}$ is *larger* than what we have estimated. Also the total accretion power is larger, and it is sufficient to explain the large jet power we have derived. Assume that the total power extractable from the accretion process is $\eta_{\rm tot} \dot{M}_{\rm in} c^2$, and that a fraction $\eta_{\rm d}$ ($\eta_{\rm j}$) of $\dot{M}_{\rm in} c^2$ is used to produce the disk luminosity (the jet power). We have:

$$\begin{aligned} \eta_{\rm tot} \dot{M}_{\rm in} c^2 &= L_{\rm d} + P_{\rm j} \\ \eta_{\rm tot} \dot{M}_{\rm in} c^2 &= \eta_{\rm d} \dot{M}_{\rm in} c^2 + \eta_{\rm j} \dot{M}_{\rm in} c^2 \ \rightarrow \\ \eta_{\rm tot} &= \eta_{\rm d} + \eta_{\rm j} \end{aligned} \quad (6)$$

Our results imply i) $\eta_{\rm j} > \eta_{\rm d}$ and ii) that $\eta_{\rm j}/\eta_{\rm d} \sim$ const in different blazars to account for the observed $P_{\rm j}$–$L_{\rm d}$ correlation.

Jets powered by the black hole spin — The rotational energy of a maximally spinning black hole is 29% of the hole rest mass energy (i.e. up to $5 \times 10^{62} M_9$ erg), amply sufficient to power a strong jet for its entire lifetime. In principle, in this case one can have $P_{\rm j} > L_{\rm d}$, given a sufficiently efficient way to extract the energy of the spinning black hole. In this case we can "decouple" $P_{\rm j}$ and $L_{\rm d}$, since they have a different energy source.

On the other hand, for FSRQs, we do see a relation between the $P_{\rm j}$ and $L_{\rm d}$, and at first glance this seems to suggest that it is the accretion, not the spin, to power the jet. We can envisage a possible solution to this apparently contradictory issue, by linking the extraction of the hole rotational energy to the accretion process. The main idea is the following: the energy density $\rho_0 v_\psi^2$ of the accreting material close to the black hole horizon can sustain a maximum magnetic energy density $B_0^2/(8\pi)$ of the same order (see also Ghisellini & Celotti 2002). Here v_ψ is the circular (keplerian) velocity of the matter. The magnetic field sustained by the accreting matter can then tap the rotational energy of the hole. The mechanism able to do this task is the Blandford–Znajek (1977) process (hereafter BZ), whose efficiency has been debated in recent years (e.g. Moderski & Sikora 1996; Ghosh & Abramowicz 1997; Livio, Ogilvie & Pringle 1999; McKinney 2005; Garofalo 2009; Krolik & Hawley 2002). Here, for simplicity, without entering in the technical discussion on the efficiency of this mechanism, we assume that the jet power is of the form:

$$P_{\rm j} \sim k a^2 \pi R_0^2 \frac{B_0^2}{8\pi} c \quad (7)$$

where $a \leqslant 1$ is the dimension–less angular momentum of the hole, R_0 is some fiducial distance of the order of the black hole horizon, and B_0 is the magnetic field at that radius. Eq. 7 is nothing else than a Poynting flux. The factor k includes our uncertainties about the efficiency of the BZ process.

Assume that at a distance R_0 from the black hole, the disk has a height H_0 above the equatorial plane. If $v_{\rm r}$ is the radial in–fall velocity, we have

$$\dot{M}_{\rm in} = 4\pi R_0 H_0 \rho_0 v_{\rm R} \rightarrow \rho_0 = \frac{\dot{M}_{\rm in}}{4\pi R_0 H_0 v_{\rm R}} \quad (8)$$

If the energy density of the magnetic field is a fraction $\epsilon_{\rm B}$ of the kinetic energy density of the matter orbiting around the black hole, we have

$$\frac{B_0^2}{8\pi} = \frac{1}{2} \epsilon_{\rm B} \rho_0 v_\phi^2 \quad (9)$$

If a magnetic field with the same magnitude is threading the spinning hole, then we have

$$P_{\rm j} \sim \frac{\dot{M}_{\rm in} c^2 \epsilon_{\rm B} k a^2}{8(H_0/R_0)} \frac{\beta_\phi^2}{\beta_{\rm R}} = L_{\rm d} \frac{\epsilon_{\rm B} k a^2}{8\eta (H_0/R_0)} \frac{\beta_\phi^2}{\beta_{\rm R}} \quad (10)$$

Close to the gravitational or Schwarzschild radius, we may set $H_0/R_0 \lesssim 1$. The ratio $\beta_\phi^2/\beta_{\rm R}$ can be slightly larger than unity, depending on viscosity. For $\epsilon_{\rm B} \sim 1$, the jet power is maximum, and for k not much less than unity can be of the same order of the disk luminosity. The (rather strong) requirement that our data are posing on the BZ mechanism is therefore on its efficiency, that must be large.

ACKNOWLEDGMENTS

This work was partly financially supported by a 2007 COFIN–MIUR and an ASI I/088/06) grant. This research made use of the NASA/IPAC Extragalactic Database (NED) which is operated by the Jet Propulsion Laboratory, Caltech, under contract with the NASA. We acknowledge the use of public data from the *Swift* data archive. The research made use of data obtained from the High Energy Science Archive Research Center (HEASARC), provided by NASA's GSFC.

REFERENCES

Abdo A.A., Ackermann M., Ajello M., et al., 2009a, ApJ, 700, 597 (A09)
Abdo A.A., Ackermann M., Ajello M., et al., 2009b, ApJ, 699, 976
Aharonian F., Akhperjanian A.G., Razer–Bachi A.R. et al., 2007, ApJ, 664, L71
Albert J., et al., 2007, ApJ, 669, 862
Barth A.J., Ho L.C. & Sargent W.L.W., 2003, ApJ, 583, 134
Blandford R.D. & Znajek R.L., 1977, MNRAS, 179, 433
Błazejowski M., Sikora M., Moderski R. & Madejski G.M., 2000, ApJ, 545, 107
Böttcher M. & Dermer C.D., 2002, ApJ, 564, 86
Cardelli J.A., Clayton G.C. & Mathis J.S., 1989, ApJ, 345, 245
Cavaliere A. & D'Elia V., 2002, ApJ, 571, 226
Celotti A. & Ghisellini G., 2008, MNRAS, 385, 283
Chen Z., Gu M., Fan Z. & Cao X., 2009, Research in Astr. Astrophys., in press (astro–ph/0906.3373)
Falomo R., Kotilainen J.K., Carangelo N. & Treves A., 2003a, ApJ, 595, 624
Falomo R., Carangelo N. & Treves A., 2003b, MNRAS, 343, 505
Fichtel C.E., Bertsch J., Chiang J. et al., 1994, ApJS, 94, 551
Foschini L. et al. 2009, Proceedings of the Conference "Accretion and Ejection in AGN: a global view", in press (astro–ph/0908.3313)
Fossati G., Maraschi L., Celotti A., Comastri A. & Ghisellini G., 1998, MNRAS, 299, 433
Garofalo D., 2009, ApJ, 699, 400
Georganopoulos M. & Kazanas D., 2003, ApJ, 594, L27
Ghisellini G., Celotti A., Fossati G., Maraschi L. & Comastri A., 1998, MNRAS, 301, 451

Ghisellini G. & Celotti A., 2001, MNRAS, 327, 739
Ghisellini G. & Celotti A., 2002, in "Blazar Astrophysics with BeppoSAX and Other Observatories" workshop, Editors: P. Giommi, E. Massaro, G. Palumbo. ESA–ESRIN, p. 257.
Ghisellini G. & Tavecchio F., 2008, MNRAS, 386, L28
Ghisellini G., Foschini L., Volonteri M., Ghirlanda G., Haardt F., Burlon D., Tavecchio F. 2009a, MNRAS, 399, L24
Ghisellini G., Tavecchio F., Bodo G. & Celotti A., 2009b, MNRAS, 393, L16
Ghisellini G., Maraschi L. & Tavecchio F., 2009, MNRAS, 396, L105
Ghisellini G., Tavecchio F. & Ghirlanda G., 2009, MNRAS, in press (Paper 1)
Ghisellini G. & Tavecchio F., 2009, MNRAS, 397, 985 (GT09)
Ghosh P. & Abramowicz M.A., 1997, MNRAS, 292, 887
Giannios D., Uzdensky D.A. & Begelman M.C., 2009, MNRAS, 395, L29
Ho L., 2008, ARA&A, 46, 475
Ho L., 2009, ApJ, 699, 626
Jauncey D.L., Savage A., Morabito D.D., Preston R.A., Nicolson G.D. & Tzioumis A.K. 1989, AJ, 98, 54
Jolley E.J.D. & Kuncic Z., 2008, MNRAS, 386, 989
Jolley E.J.D., Kuncic Z., Bicknell G.V. & Wagner S., 2009, MNRAS, in press (astro–ph/0908.2337)
Kalberla P.M.W., Burton W.B., Hartmann D., Arnal E.M., Bajaja E., Morras R. & Pöppel W.G. L. 2005, A&A, 440, 775
Kataoka J., Stawarz Ł., 2005, ApJ, 622, 797
Kataoka J., et al., 2008, ApJ, 685, 839
Krolik J.H. & Hawley J.F., 2002, ApJ, 573, 754
Liu Y., Jiang D.R. & Gu F., 2006, ApJ 637, 669
Liu Y., Jiang D.R. & Gu M.F., 2009, ApJ, 637, 669
Livio M., Ogilvie G.I. & Pringle J.R., 1999, ApJ, 512, 100
Maraschi L. & Tavecchio F., 2003, ApJ, 593, 667
McKinney J.C., 2005, ApJ, 630, L5
Moderski R. & Sikora M., 1996, MNRAS, 283, 854
Padovani P., 1992, A&A, 256, 399
Piner B.G. & Edwards P.G., 2004, ApJ, 600, 115
Piner B.G., Pant N. & Edwards P.G., 2008, ApJ, 678, 64
Pian E., Falomo R., & Treves A., 2005, MNRAS, 369, 919
Poole T.S., Breeveld A.A., Page M.J. et al., 2008, MNRAS, 383, 627
Roming P.W.A., Kennedy T.E., Mason K.O., et al., 2005, Space Sci. Rev., 120, 95
Sambruna R.M., Gliozzi M., Tavecchio F. et al., 2006, ApJ, 652, 146
Schlegel D.J., Finkbeiner D.P. & Davis M., 1998, ApJ, 500, 525
Shakura N.I. & Syunyaev, R.A., 1973, A&A, 24, 337
Sikora M., Begelman M.C. & Rees M.J., 1994, ApJ, 421, 153
Sikora M., Błazejowski M., Moderski R. & Madejski G.M., 2002, ApJ, 577, 78
Tavecchio F., Maraschi L. & Ghisellini G., 1998, ApJ, 509, 608
Tavecchio F., Maraschi L., Sambruna R.M., Urry C.M., Cheung C.C., Gambill J.K. & Scarpa R., 2004, ApJ, 614, 64
Tavecchio F., Maraschi L., Ghisellini G., Kataoka J., Foschini L., Sambruna R.M. & Tagliaferri G., 2007, ApJ, 665, 980
Tavecchio F., Ghisellini G., Ghirlanda G., Foschini L. & Maraschi L., 2009, MNRAS, in press (astro–ph/0909.0651) (T09)
Vlahakis N. & Königl A., 2004, ApJ, 605, 656
Wagner R.M., 2008, MNRAS, 385, 119
Wang J–M., Luo B. & Ho L.C., 2004, ApJ, 615, L9
Woo J–H., Urry C.M., van der Marel R.P., Lira P. & Maza J., 2005, ApJ, 631, 762
Worrall D.M., Birkinshaw M. & Hardcastle M.J., 2001, MNRAS, 326, L7
Wu X.–B., Liu F.K. & Zhang T.Z., 2002, A&A 389, 742
Xie G.Z., Liu H.T., Cha G.W., Ma L., Xie Z.H. & Chen L.E., 2005, AJ 130, 2506
Xu Y.-D., Cao X. & Wu Q., 2009, ApJ, 694, L107

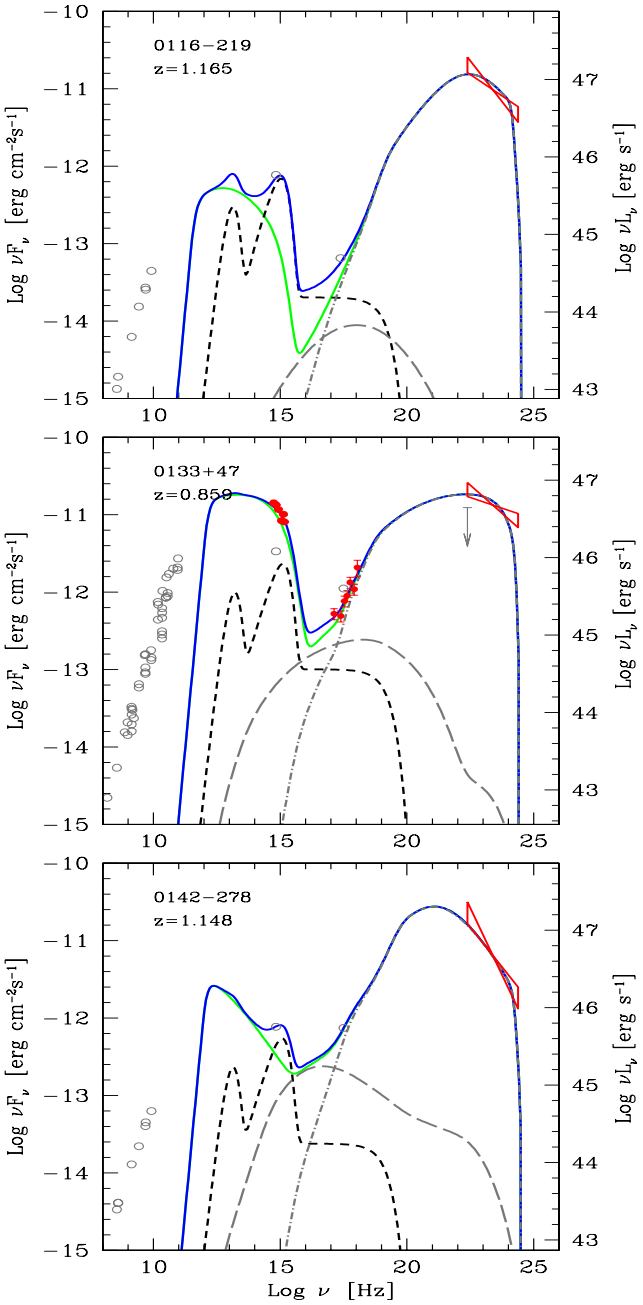

Figure 11. SED of PKS 0166–219, 0133+47 (DA 55) and PKS 0142–278, together with the fitting models, with parameters listed in Tab. 4. *Fermi* and *Swift* data are indicated by dark grey symbols (red in the electronic version), while archival data (from NED) are in light grey. The short–dashed line is the emission from the IR torus, the accretion disk and its X–ray corona; the long–dashed line is the SSC contribution and the dot–dashed line is the EC emission. The solid light grey line (green in the electronic version) is the non thermal flux produced by the jet, the solid dark grey line (blue in the electronic version) is the sum of the non–thermal and thermal components.

10 APPENDIX: SPECTRAL ENERGY DISTRIBUTIONS

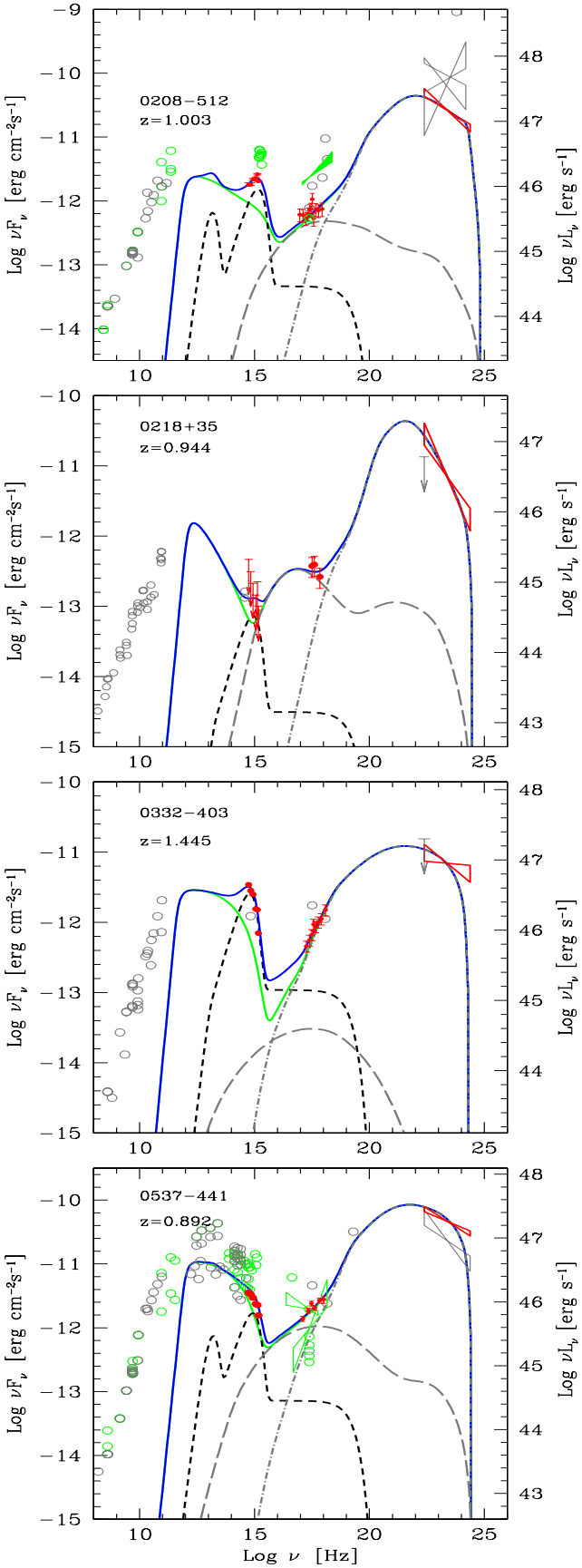

Figure 12. SED of PKS 0208–512, B2 0218+35, PKS 0332–403 and PKS 0537–441. Symbols and lines as in Fig. 11.

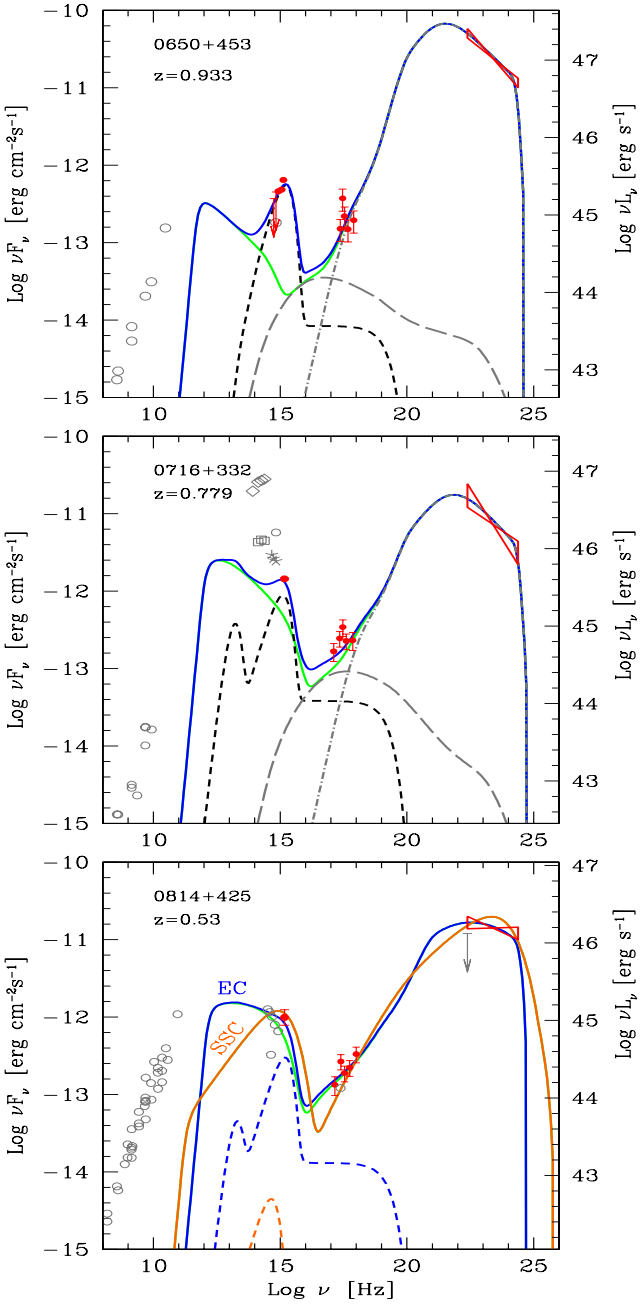

Figure 13. SED of B3 0650+453, TXS 0716+332 and 0814+425 (OJ 425). For the latter source we show a pure SSC model and an EC one, as indicated. Symbols and lines as in Fig. 11.

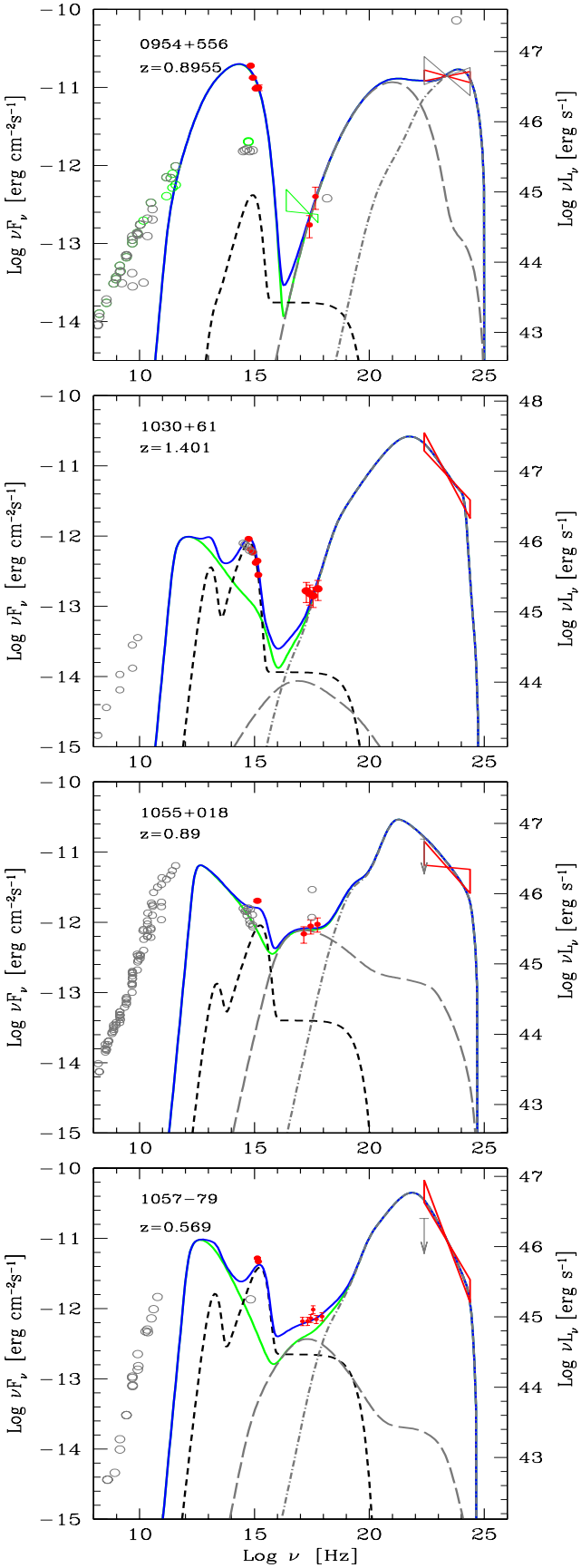

Figure 14. SED of 0954+556 (4C 55.17), S4 1030+61, PKS 1055+018 and PKS 1057–79. Symbols and lines as in Fig. 11.

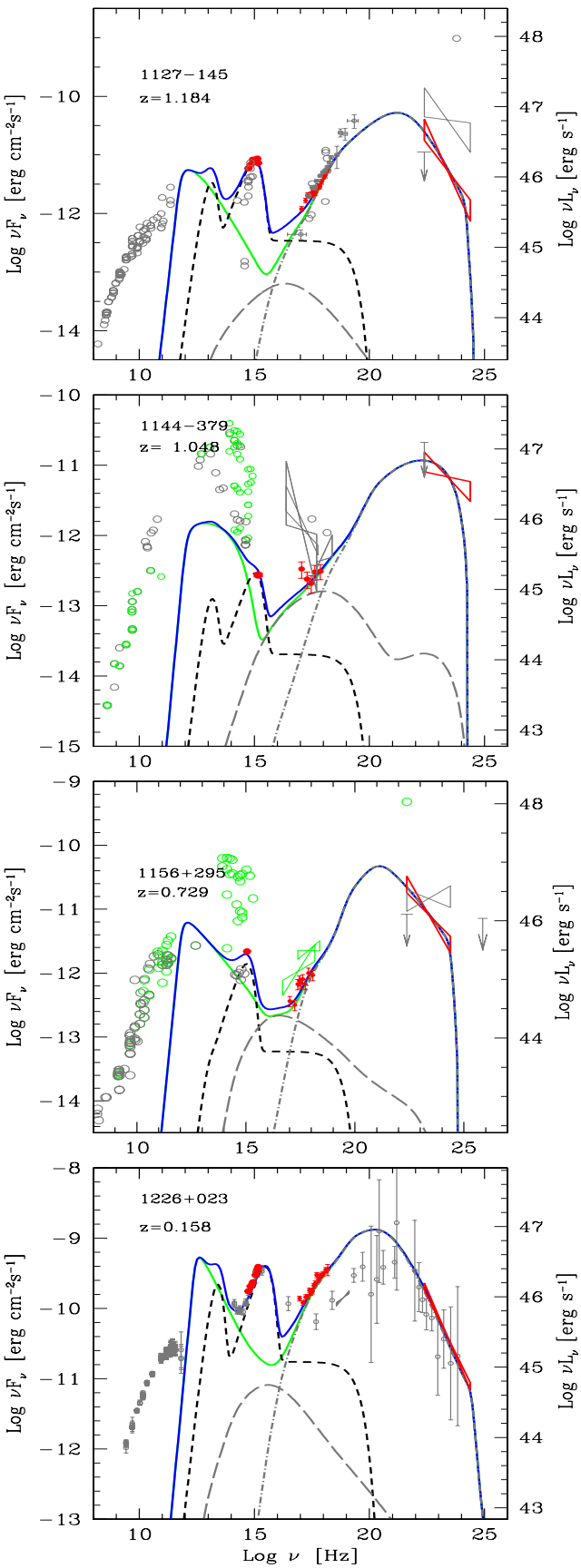

Figure 15. SED of PKS 1127–145, PKS 1144–379, 1156+295 (4C 29.45) and 1226+023 (3C 273). Symbols and lines as in Fig. 11.

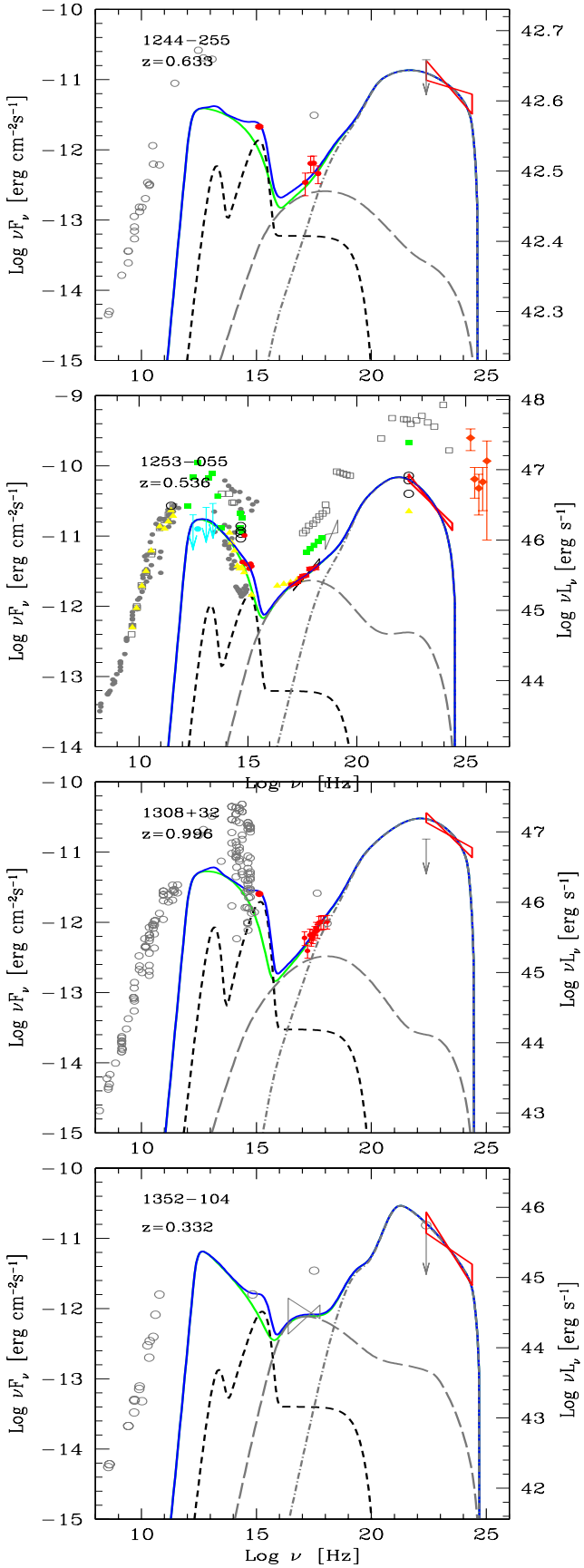

Figure 16. SED of PKS 1244–255, 1253–055 (3C 279), B2 1308+32 and PKS 1352–104. Symbols and lines as in Fig. 11.

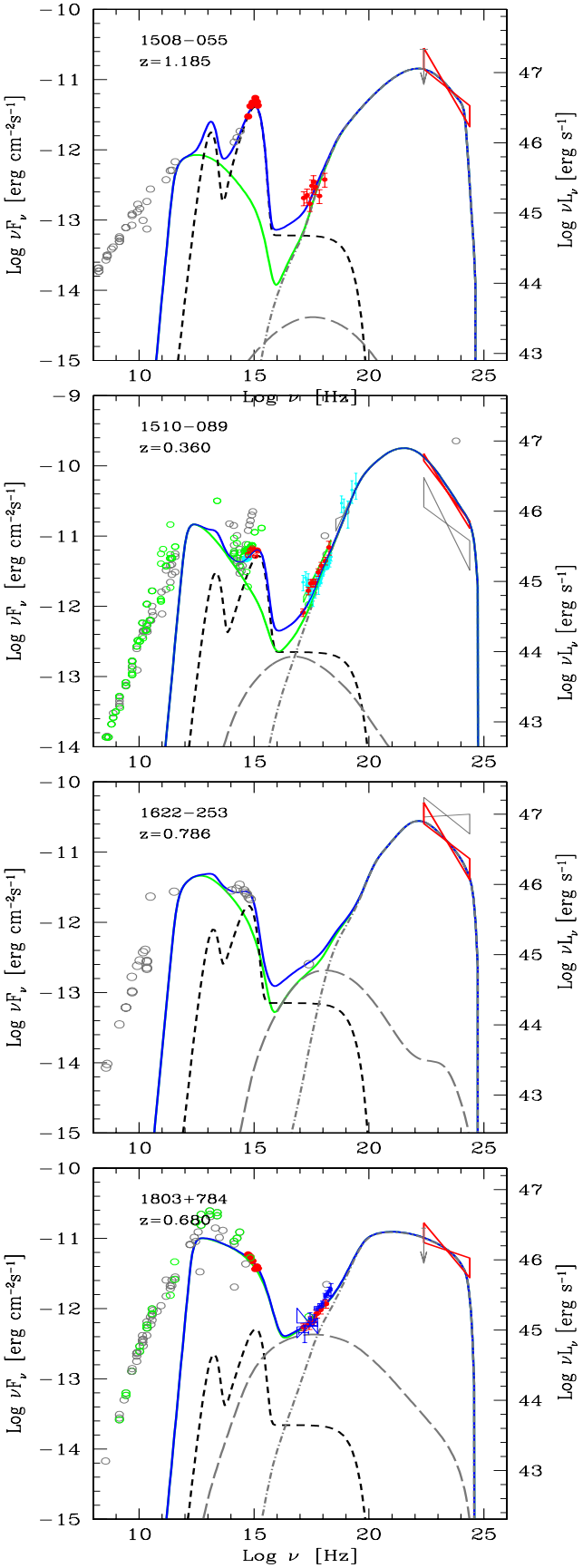

Figure 17. SED of PKS 1508–055, PKS 1510–089, PKS 1622–253 and S5 1803+784. Symbols and lines as in Fig. 11.

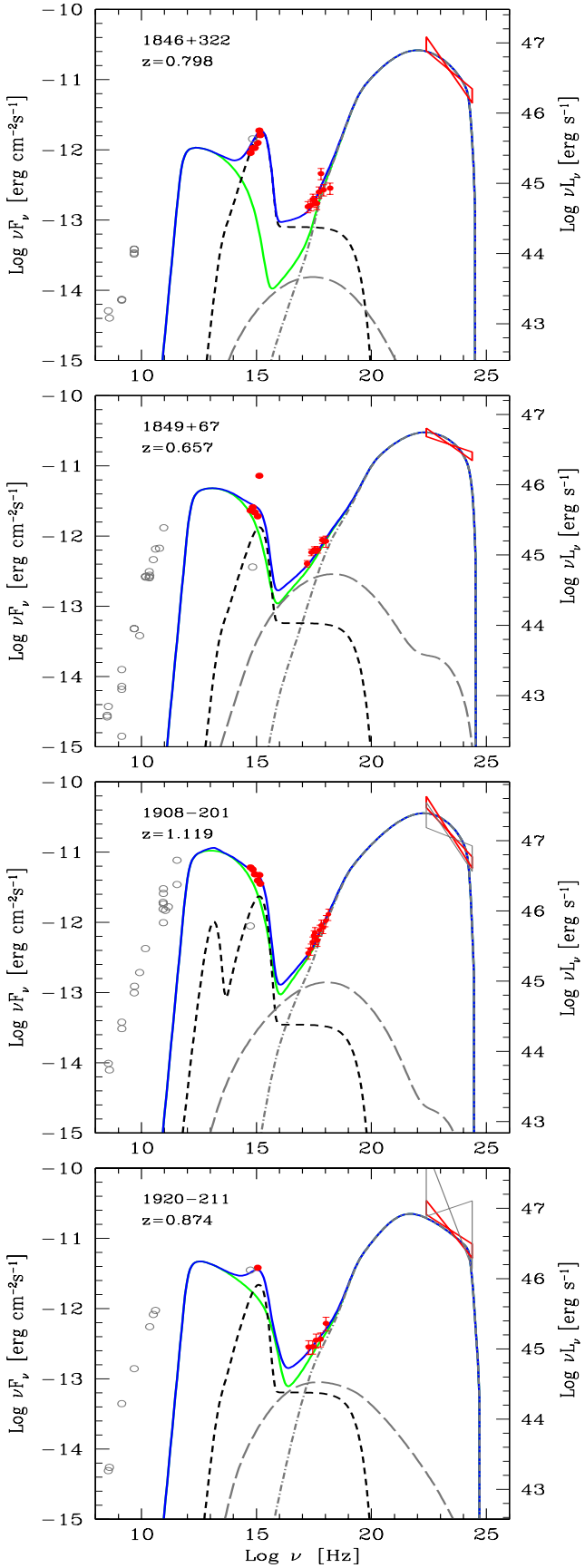

Figure 18. SED of TXS 1846+322, S4 1849+67, PKS 1908–201 and TXS 1920–211. Symbols and lines as in Fig. 11.

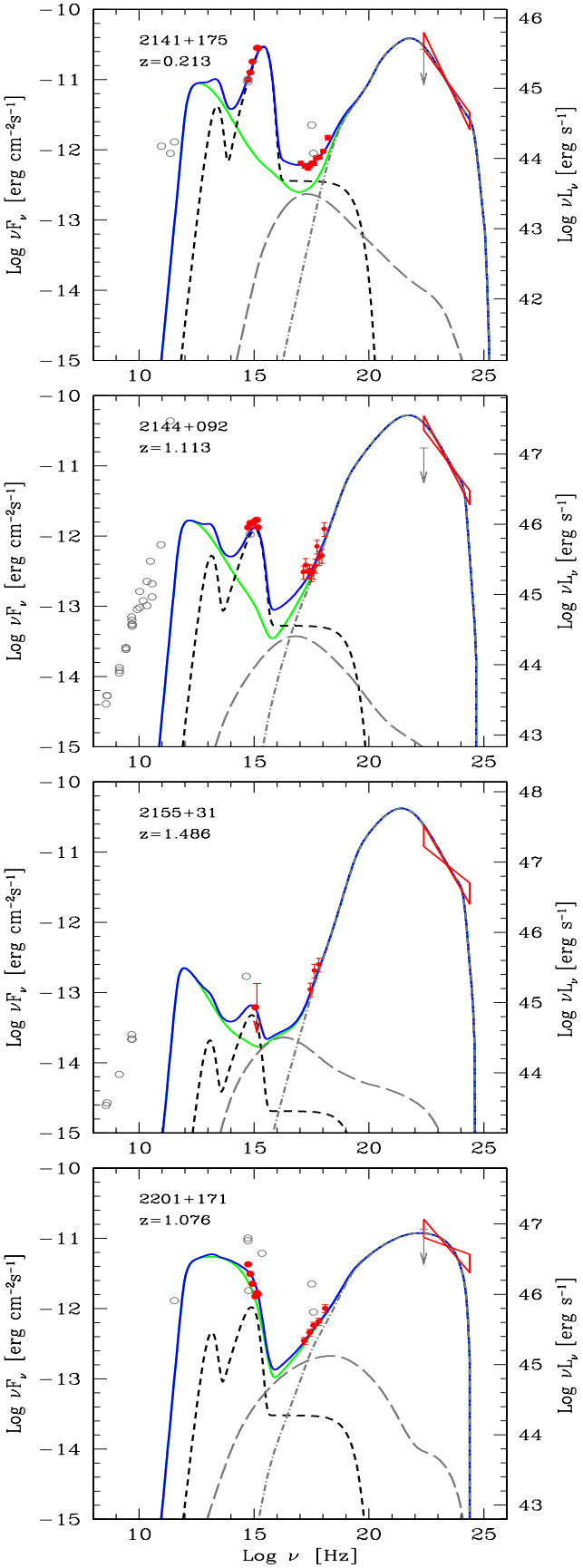

Figure 19. SED of 2141+175 (OX 169), PKS 2144+092, B2 2155+31 and PKS 2201+171. Symbols and lines as in Fig. 11.

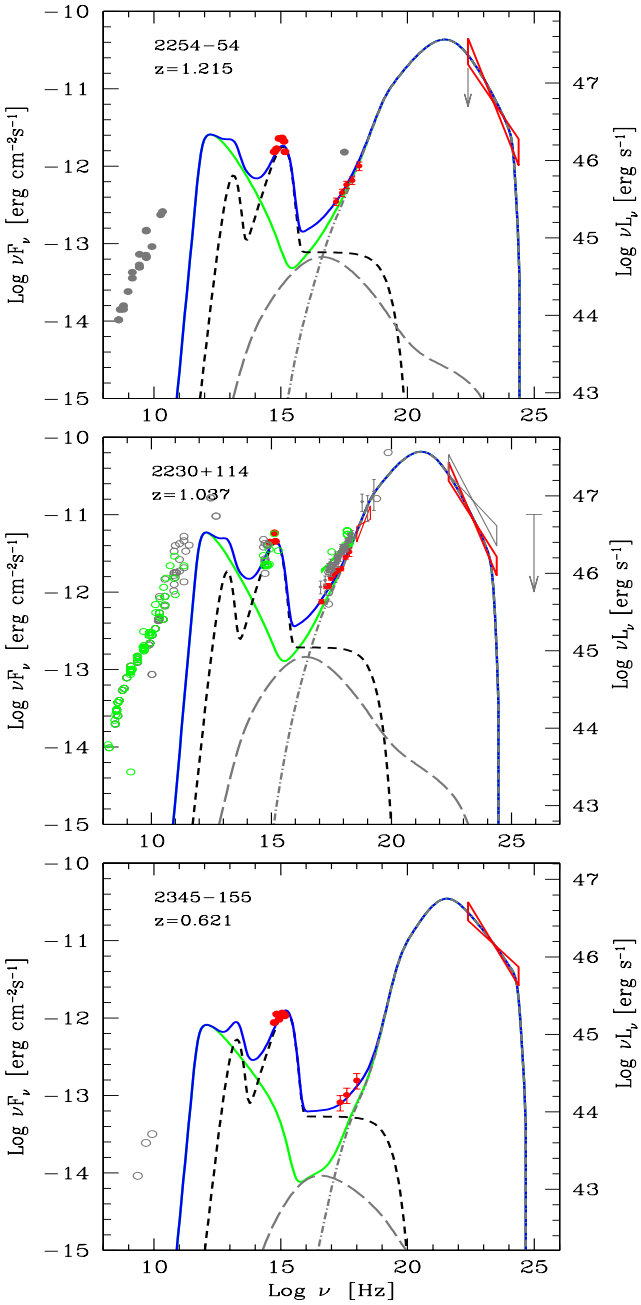

Figure 20. SED of PKS 2204–54, 2230+114 (CTA102) and PMN 2345–1555. Symbols and lines as in Fig. 11.